AUTOMATED SYSTEM FOR THE CHARACTERIZATION

OF THE BIOMECHANICAL PROPERTIES

OF HUMAN SOFT TISSUE

by

MICHAEL ABRAHAM, MS

Presented to the Faculty of the Graduate School of

The University of Texas at Arlington in Partial Fulfillment

of the Requirements

for the Degree of

MASTER OF SCIENCE IN MECHANICAL ENGINEERING

THE UNIVERSITY OF TEXAS AT ARLINGTON

August 2016

Dedicated to my Parents,
who worked too hard, traveled too far, and bore too heavy
for my education and my future

Acknowledgements

Abstract

AUTOMATED SYSTEM FOR THE CHARACTERIZATION

OF THE BIOMECHANICAL PROPERTIES

OF HUMAN SOFT TISSUE

Michael Abraham, MS

The University of Texas at Arlington, 2016

Supervising Professor: Panayiotis S. Shiakolas

Vaginal prolapse is a common condition that affects a large number (approximately 3.3 million in the US) of women, mainly above the age of 50 years. The condition is characterized by the weakening and breakdown of the pelvic support structures such as muscles and connective tissues, leading to the dislodging and prolapse of pelvic organs. Current examinations of the pelvic tissue are manually performed by the physician who assesses its rigidity. These exams are subjective and offer qualitative rather than quantitative results of the state of the pelvic tissue. In this research, a complete system was conceptualized and designed to assess the biomechanical properties of the anterior vaginal wall in-vivo. The design mimics the palpating action performed by the physician on the vaginal wall

to sense its rigidity. The reaction force profile resulting from the palpation is recorded and curve-fit to characterize the viscoelastic properties of the vaginal tissue. The data can later be used to provide a quantitative measure for the onset and progression of a condition by tracking the viscoelastic properties of the tissue.

Considerations were taken into account to accommodate the environment constraints. Different sensing, actuation, and control technologies were explored and revised to improve the design. Finite element analysis (FEA) was performed to verify the structural safety of the hardware components. The system is controlled using National Instruments (NI) LabVIEW software and a NI myRIO controller. Additionally, a graphical user interface (GUI) in LabVIEW was developed and integrated to ease the operation of the device by a physician for in-vivo testing. The system was used to collect an initial sample set of in-vivo data from patients to verify the operational function of the prototyped system and identify areas in need of improvement.

Table of Contents

List of Illustrations

List of Tables

Chapter 1

INTRODUCTION

<u>Pelvic Organ Prolapse</u>

Pelvic organ prolapse (POP) is a common condition affecting a large number of women per year. It is a result of the weakening of support for the pelvic organs such as the uterus, bladder, or colon. Consequently, the female pelvic organs prolapse (descend) and push against the vaginal walls as seen in Figure 1.1. In some cases, severe POP may result in the protrusion of the pelvic organs or vaginal walls outside of the body [1]. This condition is so prevalent that a 2009 study estimates that the number of women affected by POP is approximately 3.3 million; and this number is expected to rise 46% by 2050 due to the aging population of baby boomers [2]. An American female has an 11.1% lifetime risk of undergoing an operation for pelvic organ prolapse at the age of 80 [3], and 75% of patients aged 18 to 83 presenting for a routine gynecological examination show some level of loss of vaginal or uterine support [4]. The condition is especially more common in older age groups (50 years and older). Patients of POP experience pain, urinary incontinence, difficulty of intercourse, impediment of motion, and a general decline in positive body image.
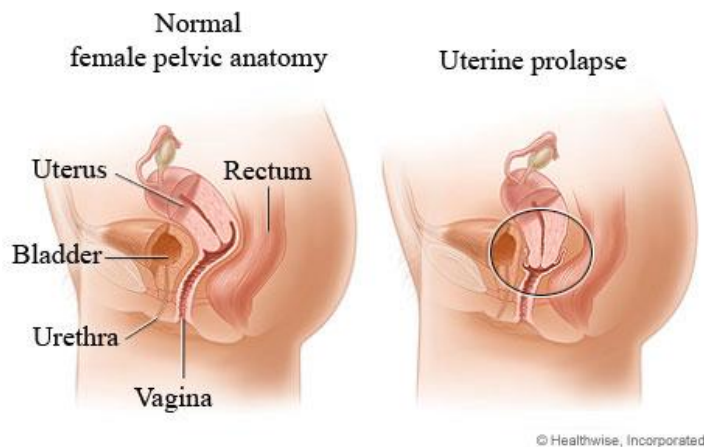
Figure 1.1 Normal pelvic anatomy (left) and prolapsed uterus (right) [5]

The risk of prolapse can be attributed to a number of factors such as aging, childbirth, obesity, smoking, chronic straining, etc. However, the development of POP is thought to be brought on by a change in the biomechanical properties of the pelvic muscles and connective tissues [6]. The anterior vaginal wall (AVW) is one of the regions that is most affected by this condition. Physicians in general, urologists in particular, assess this change in AVW biomechanical properties using a traditional pelvic exam, similar to the digital rectal exam performed to diagnose prostate enlargement in males. However, such tests are inherently subjective and qualitative in nature, with no measurable or comparable data across patients and physicians. Therefore, research is active in the area of testing and studying the biomechanical properties of the vaginal tissue of women with pelvic organ prolapse in-vivo.

<p style="text-align:center"><u>Prior art in Biomechanical Testing of Soft Tissue</u></p>

Multiple experiments have been conducted for the testing and modeling of the biomechanical properties of soft tissue in general, and vaginal tissue in particular. Many of these experiments are conducted ex-vivo on tissue samples and organs extracted from patients or cadavers, while others are conducted during surgery on the exposed organs. Experiments can be categorized in many different ways: testing method (indentation, aspiration, etc.), testing condition (i.e. in-vivo or ex-vivo), and mechanical model type (elastic, viscoelastic, hyperplastic, etc.). For the purpose of this research, the most relevant categorization is the one based on the testing method. Three major testing methods were identified in the literature: indentation, aspiration, and rheometry.

Indentation tests in particular are of most interest to this thesis research. Carter *et al*. used an indenter equipped with a load cell to obtain stress-strain curves from human and porcine liver

[7]. Their experiments on human subjects were conducted on patients undergoing surgery. Miller *et al.* also used a load cell equipped indenter to generate the force-displacement curves on a pig brain in-vivo [8]. Additionally, they used magnetic resonance imaging (MRI) to generate the indentation deformation, and solve numerically for the force-displacement response. A similar concept to Miller's was also conducted by Ahn using an indenter and a deformation analyzer camera using extracted porcine liver [9]. Other studies such as the ones by Liu [10] [11], Samur [12], and Tay [13] also employ the same indentation tools whether in-vivo or ex-vivo. It is important to note the variations in biomechanical models used between experiments. Some studies employed non-linear hyperplastic models while others used different kinds of viscoelastic models.
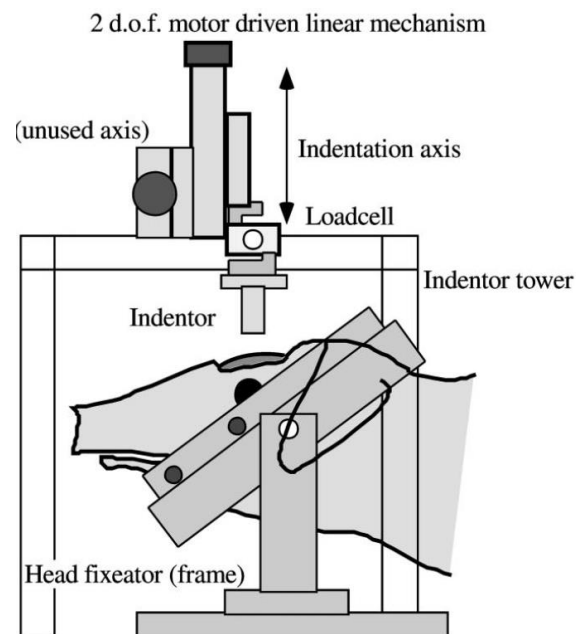
Figure 1.2 – Schematic setup of an in-vivo indentation experiment on swine brain [7]

When studying vaginal tissue specifically, most studies are performed ex-vivo due to the difficulty of accessing the vaginal tissue in-vivo with sufficient testing reliability. Cosson *et al.* performed tests on extracted human vaginal tissue using an indentation method similar to the

aforementioned studies. The study indented the stretched vaginal tissue using a piston up to rupture while recording the indentation force; it also measured the force required to rupture a suture [14]. Peña *et al*. performed uniaxial tensile tests on extracted vaginal tissue in an attempt to characterize the non-linear softening behavior of the tissue [15]. Similarly, Rubod *et al*. also performed a series of uniaxial tensile tests on extracted tissue (see Figure 1.3), and again arrived at a non-linear characterization of the stress-strain relation of the tissue [16]. Many of these experiments were done specifically for the purpose of observing biomechanical changes in cases of pelvic organ prolapse.
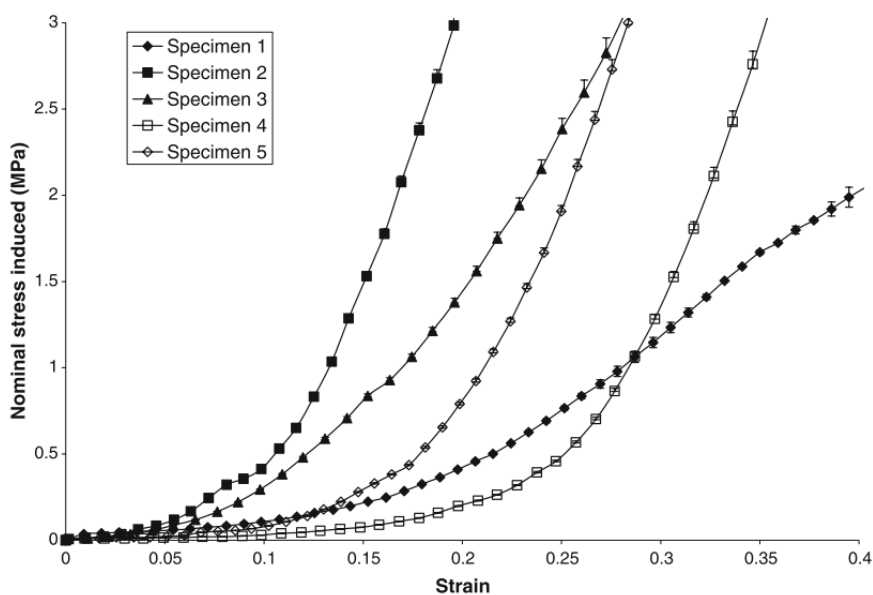
Figure 1.3 – Stress–strain curves obtained for uniaxial tension test on prolapsed tissues obtained on five different patients [16]

While these experiments provide a closer examination of the tissue properties and definitely improve the understanding of the biomechanical changes that accompany the POP condition, they are unavoidably limited by the need to extract live tissue from the patient or the need for operative surgery to access the internal organs. Such limitations pose a real challenge to

the employment of tissue biomechanical properties as a measure of pelvic organ prolapse. There's a clear need for quantitative in-vivo test data that is also easy to acquire in a minimally or non-invasive repeatable approach.

<div align="center">Prior Art in in-vivo Testing of Vaginal Tissue</div>

A literature and patent search concluded that there's a limited number of devices available to accommodate such need. In a paper published by Chuong *et al*. [6], the researchers inserted a probe with a 10mm circular orifice onto the anterior vaginal wall (AVW), see Figure 1.4. Suction was applied on the orifice to uplift the vaginal tissue and then released to relax it. Laser altimetry was used to determine the rate of both the uplift and relaxation of the tissue. The uplift versus time test data was then curve-fit using the Voight model to produce the viscoelastic time constant of the tissue.

While the recorded data does produce a quantitative measure of tissue stiffness, the device does have some limitations. Namely, the use of suction pressure requires the direct contact between the device and the vaginal wall, which in turn creates the need for repeated sterilization. Portability is also hindered by the need to either keep the device within the reach of a vacuum source or attaching one to it.

Another device produced by Advanced Tactile Imaging Inc. uses a probe with an array of pressure sensors and an accelerometer to map a pressure image of the vaginal wall, see Figure 1.5 A [17]. The device is operated manually, as the user orients and pushes the probe to indent the vaginal tissue as desired. Unlike the experiment created by Chuong el al, this device does not produce an individual or multiple indicators (such as a viscoelastic constant) to characterize the

<div align="center">5</div>

tissue biomechanical properties. Instead, it produces what they describe as a tactile image shown in Figure 1.5 B [17].
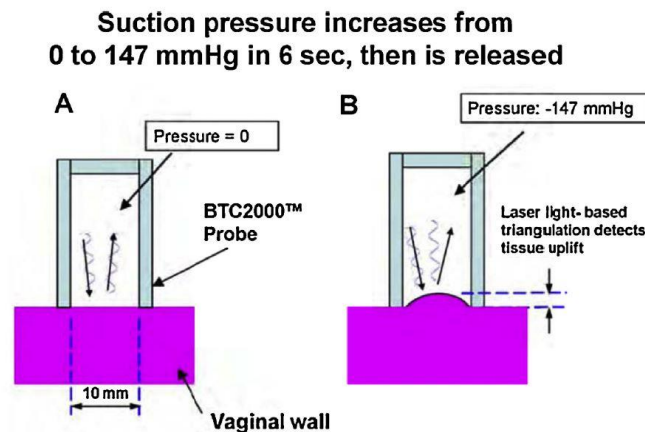
Figure 1.4 – BTC2000^{TM} laser altimetry device used in study by Chuong *et al*. [6]

The tactile image produced by the VTI device does provide insight into the biomechanical state of the tissue. However, this technology, similar to ultrasound and MRI, produces a more qualitative, rather than quantitative, measure to the biomechanical properties of the vaginal wall.

The tactile image produced by the VTI device does provide insight into the biomechanical state of the tissue. However, this technology, similar to ultrasound and MRI, produces a more qualitative, rather than quantitative, measure to the biomechanical properties of the vaginal wall.

To the extent of the author's knowledge, there is no technology readily available to assist in evaluating the biomechanical properties of vaginal tissue in-vivo and in-office with relative ease and repeatability. The objective of this research was the development of a novel device to meet the aforementioned need for such tests, while avoiding some of the limitations of currently available devices.
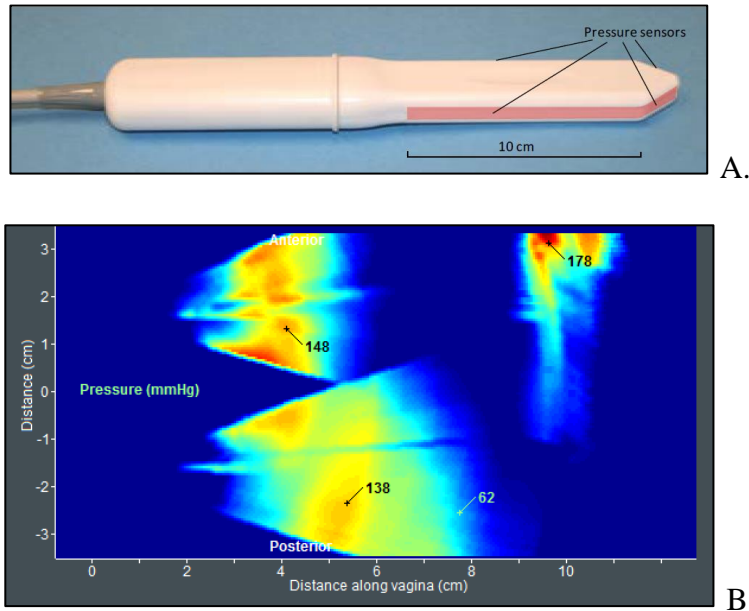
Figure 1.5 – A. The Vaginal Tactile Imager (VTI) developed by Advanced Tactile Imaging Inc.

– B. A tactile image produced by the VTI [17]

Prior Art in Mechanical Finger Technology

In their own regard, mechanical hands are in no way a novel or recent technology. Research in the fields of prosthetics, robotics, and haptics has been investigating mechanical hands for decades. For example, a 1917 US patent proposed the design of an artificial hand actuated by tendons [18] – a concept still used today for many modern mechanical hands. Nonetheless, in recent years many advancements have been made, especially in the methods of actuation, control, force sensing and haptic feedback.

In terms of force/pressure sensing, there are multiple sensing methods that have been developed and implemented in artificial hands such as capacitive, strain gauges, piezoresistive, and optical sensors. Capacitive sensors consist of two layers of a conductive material separated by a dielectric. When the layers are compressed and move relative to each other, the capacitance changes. The change in capacitance can be read and calibrated in to a force reading. Capacitive

sensors generally offer excellent repeatability and high resolution; however, they are more susceptible to interference and noise and thus require complex noise-filtration electronics.

Multiple designs of capacitive sensors have been synthesized and tested over the past decade. Brookhuis *et al*. created a capacitive sensor for 3D force sensing using 144 silicon pillars as the top electrode and a flat plate as the bottom electrode. Four quadrants are being read, and the force location and direction can be registered depending on the differential capacitance change between quadrants [19]. Another design by Liang *et al*. consists of two electrodes separated by a layer of PDMS pyramid array, see Figure 1.6. The sensor is intended to be flexible and also capable of 3D force sensing [20].
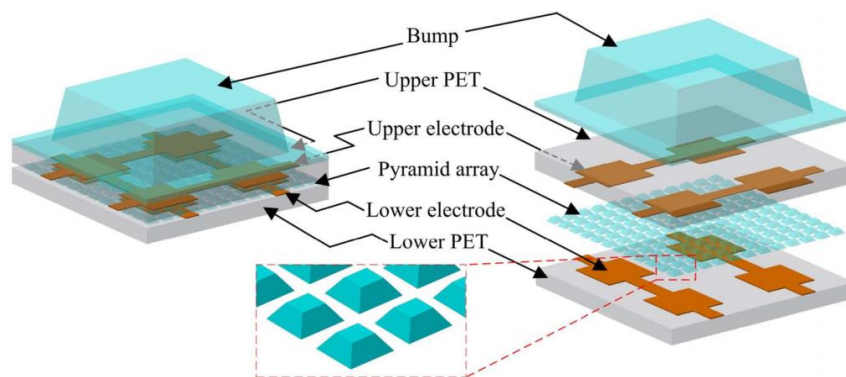
Figure 1.6 - Flexible capacitive tactile sensor array with truncated pyramids as dielectric layer for three-axis force measurement by Liang *et al*. [20]

Another sensor technology is piezoresistive sensors. They consist of a material which changes resistance when subjected to pressure. Piezoresistive sensors typically have high resolution and are easily integrated, however they can suffer from a slow non-linear response, hysteresis, and also susceptible to fatigue and permanent deformation. An example of the technology has been designed and prototyped by Jung *et al*. who developed a multidirectional piezoresistive sensor consisting of five sensing elements made of a Carbon Nanotubes/PDMS

composite, see Figure 1.7. The elements contact surfaces consist of microdomes whose resistance decreases drastically when compressed. The resistance change causes a change in output voltage which can be read and calibrated to correspond to specific loading conditions [21].
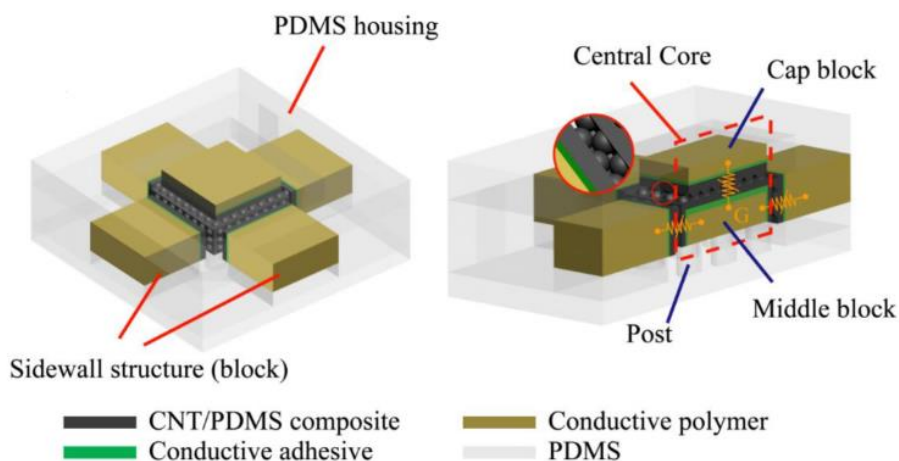
Figure 1.7 – Piezoresistive tactile sensor discriminating multidirectional forces by Jung *et al*. [21]

Strain gauge technology is another force sensing technology which has been being widely used for decades. The sensing element consists of a thin strip containing a conductive pattern. When the pattern is stretched or bent due to force/pressure, its resistance changes due to the Poisson effect, and this change can be registered and calibrated. Strain gauges offer high sensitivity, low profiles, and are generally inexpensive. Their limitations include but are not limited to susceptibility to temperature changes and hysteresis. While the technology itself is not new, recent designs incorporate strain gauges into novel configurations to enhance their functionality. Liang *et al*. designed a fingertip containing two annular diaphragms. Strain gauges were distributed around the two annular diaphragms to measure both normal and tangential forces and also tangential moments, see Figure 1.8 [22]. The decoupling of the strain gauge signals was achieved through a neural network method [22].
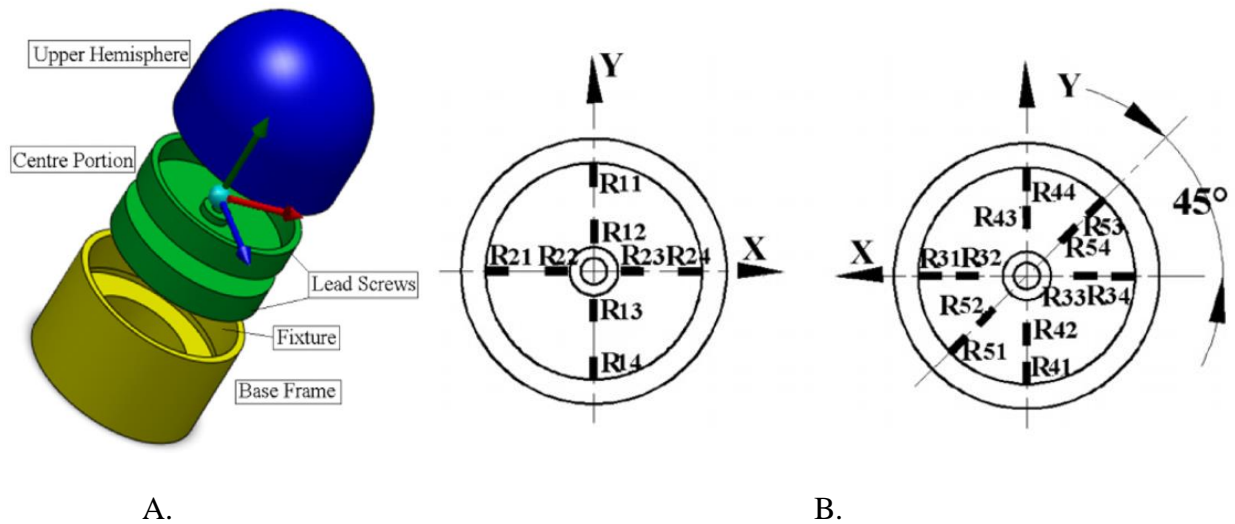
Figure 1.8 – A. Exploded view of a miniature robust five-dimensional fingertip force/torque sensor by Liang *et al*. [22] – B. Strain gauge arrangement on the upper (left) and lower (right) annular diaphragms.

Research is evidently active and there is a considerable amount of prior art related to the components of the research topic and goal discussed in this document. However, the research presented in this document is not aimed at creating an original standalone sensing, actuation, or control technology, but rather incorporate existing technologies into a complete system. Thus, the system developed in the research is otherwise original in functionality and automation as will be presented in the next section, Research Objectives.

Research Objectives

The research in this thesis attempts to develop a practical in-vivo testing instrument for the characterization of vaginal soft tissue. The main objective of the contribution to this research is to create an automated testing system; capable of performing a quick and accurate test to extract force and displacement data from the vaginal wall; and capable of automatically using this data to characterize the biomechanical properties of the vaginal tissue.

The current system prototype consists of a one-joint artificial finger, equipped with a force-sensitive resistor (FSR) to measure force, belt-driven using a DC motor, and controlled using a National Instruments myRIO controller. The design mimics the palpation action performed by a physician during a routine gynecological examination. Similar to the manual exam, the artificial finger is inserted into the vagina, actuated to controllably press on the vaginal wall, and the force produced from this pressure is sensed by the FSR. The controller coordinates the motion profile, records the force and displacement data in real-time, and processes the data to characterize the biomechanical properties of the tested tissue.

While the technologies used to create the system are not novel in their own domains, the new approach to vaginal tissue testing proposed in this research is novel in utility. The device is designed to operate similar to a human finger; the test needs to be non-invasive, quick, and comfortable for the patients; the system software and graphical user interface (GUI) are designed to be user-friendly to enable the physician (or a non-technical operator of the system) to conduct tests with relative ease.

<div align="center">Outline of Thesis</div>

Chapter 1 provided an introduction to the thesis topic and its background. It provided an overview of the pelvic organ prolapse condition, prior art in the characterization of biomechanical properties of the vaginal tissue, and devices available to accomplish this task in-vivo.

Chapter 2 discusses the system design. First, the conceptual design is described and the working constraints are discussed. Second, some of the design iterations and considerations are presented. Third, the final design, along with features and specifications are discussed. Finally, the finite element analyses (FEA) performed to verify the design are discussed.

Chapter 3 discusses the system prototyping. First, a brief overview of the Fused Deposition Modeling (FDM) prototyping process is presented. Second, the sensor of choice, its specifications, actuation, and characterization are explained. Third, the motor and its actuation are discussed. And finally, the controller and the accompanying graphical user interface are introduced and the testing procedure explained.

Chapter 4 discusses the use of the developed device for in-vivo testing and the processing of the acquired data. A description of the viscoelastic model used to curve-fit the data is provided. The data is also interpreted and analyzed, and the major observations and conclusions are presented.

Chapter 5 draws the major conclusions of the research and provides recommendations for future improvements on the existing design.

Chapter 2

SYSTEM DESIGN

Conceptual Design

The working concept of the system was proposed to mimic the pelvic exam performed by the physician in the office or clinic. As shown in Figure 2.1, in a pelvic exam, the patient assumes a specific position and the physician inserts two fingers into the vagina and palpates the vaginal wall to gage the rigidity and the positioning of the vaginal wall soft tissue.
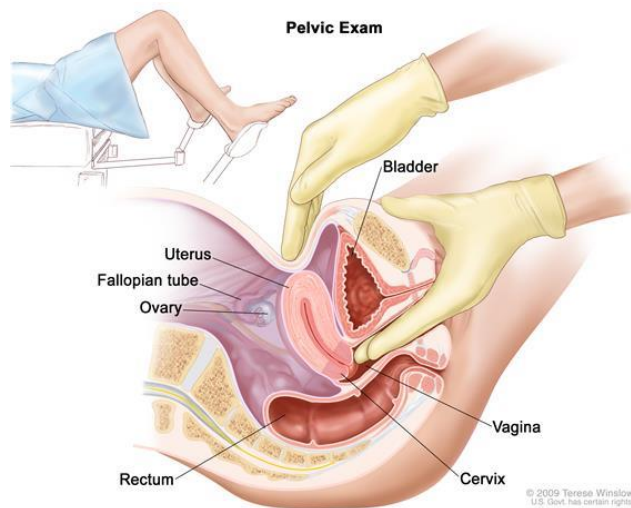
Figure 2.1 – Illustration of the pelvic exam as performed by the physician in office [23]

Therefore, a conceptual design was proposed as a probe resembling a human finger to be inserted in the vagina, and actuated to press on the vaginal wall while sensing the reaction force response. The system was conceptualized to contain the following components as shown in Figure 2.2 and operates in the following manner:

1. The User inputs the desired test parameters into the GUI, including a defined actuation profile for the Actuator.

2. The Controller activates the Actuator to perform the desired actuation profile. The Transmission method relays the actuation profile onto the soft tissue.

3. The Sensors sense the reaction force resulting from the engagement of the actuation profile, and the Controller records this force profile, as well as saves it on the local computer.

4. The Controller processes the force profile data, and presents the results to the User on the GUI.
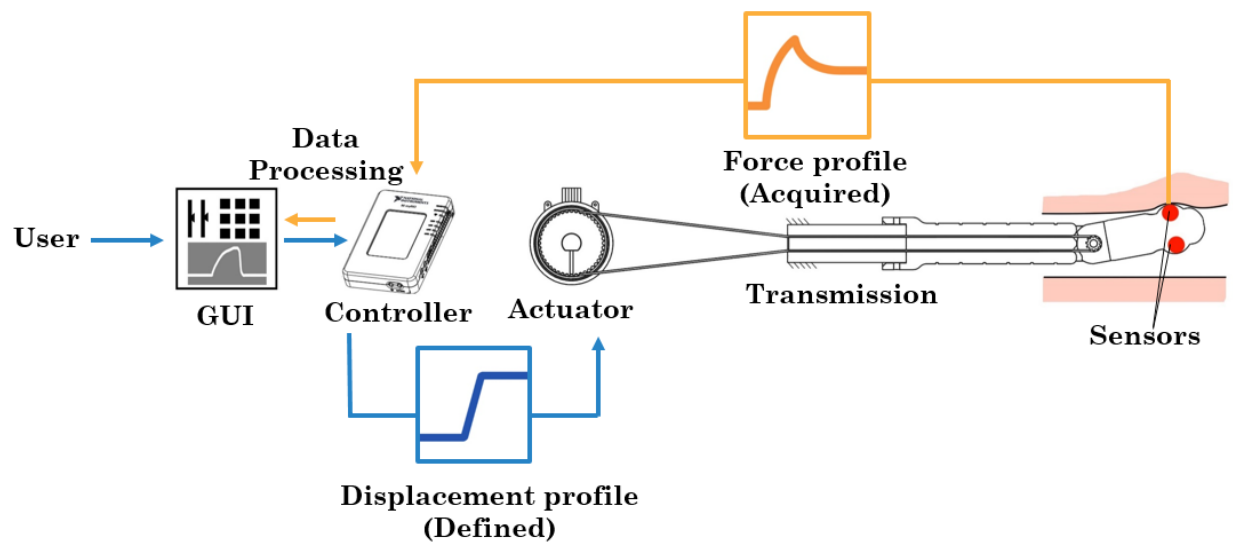
Figure 2.2 – Diagram of the different system components

Testing Environment Constraints

The device was conceptualized to resemble a human finger – a probe to be inserted into the vagina Therefore, some design constraints are enforced by the working environment. Research was performed to determine relevant constraints and considerations, to avoid discomfort to the patient or damage to the probe.
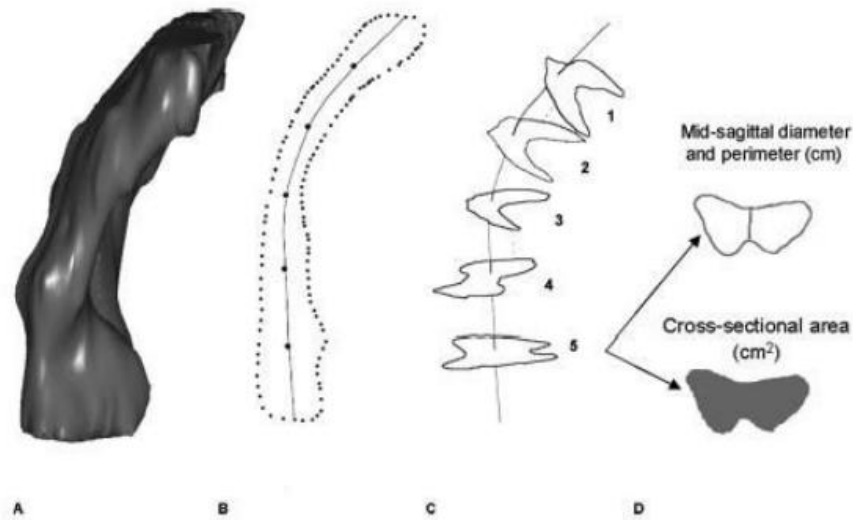
Figure 2.3 – A. Three-dimensional I-DEAS 9.0 vaginal model. B. Longitudinal axis determined in the mid-sagittal plane, with 5 equally spaced locations along the longitudinal axis marked. C. Sample cross sections: Location 1 is near the vaginal apex, and location 5 is near the hymen. D. Mid-sagittal diameter, perimeter, and cross-sectional area. By Hsu *et al*. [24]

A study performed by Hsu using Magnetic Resonance Imaging (MRI) concluded that the mean mid-sagittal diameter of the vagina is 13mm – in both women with and without prolapse [24], see Figure 2.3. Since the vaginal tissue is generally elastic and expands during intercourse and childbirth, a vaginal instrument can be relatively larger than the mean vaginal diameter. An upper limit on the diameter of 18mm was imposed – roughly the same diameter as a human male finger. The vaginal wall carries also many nerve endings near the apex of the vagina, which are sensitive to contact. Therefore, the shape and outer surfaces of the probe need to be as smooth and streamlined as possible; no sharp edges can exist; and protrusions are to be kept small and limited.

Another constraint is the chemical environment of the vagina. Since the vagina contains natural bacteria and sometimes infectious diseases, the probe needs to be easily sterilized without

sustaining damage, to prevent transmitting infections or STDs between patients. On a related note, the vagina is a humid environment containing bodily fluids, which requires the probe to be moisture and rust resistant and non-porous. Otherwise, the probe needs to be easily coverable with a plastic cover/boot when being used. This alleviates the aforementioned concerns on infection transmission and moisture. However, using a plastic cover should not hinder or affect the operation of the probe during the testing procedure.

<p align="center">Mechanical Design Process</p>

1. Original Model

The original concept of the probe design was modeled using parts of the InMoov project developed by Gael Lengavin [25]. The InMoov project provides stereolithography (STL) files to create and assemble a 3D-printed humanoid robot. The STL files for the index finger of the InMoov robot were downloaded from the InMoov website and reverse-engineered to recreate the solid model using Dassault Systèmes SolidWorks. The InMoov finger is originally designed to be actuated using tendons – wires which pull on either the anterior or the posterior sides of the finger to actuate it, as shown in Figure 2.4. However, without any modifications to this model, many of the requirements and constraints of the problem cannot be met: the motion of the finger was not reliable due to the loss of tension in the tendons; the model contained many sharp edges; and there was no location to mount sensors.
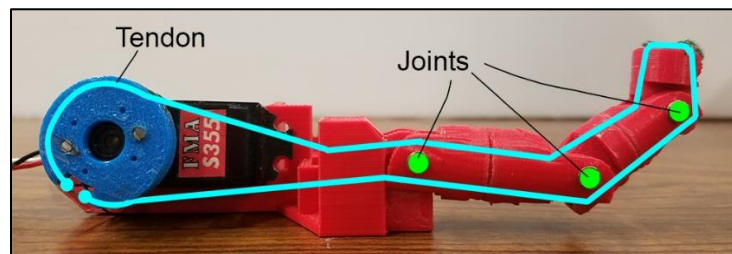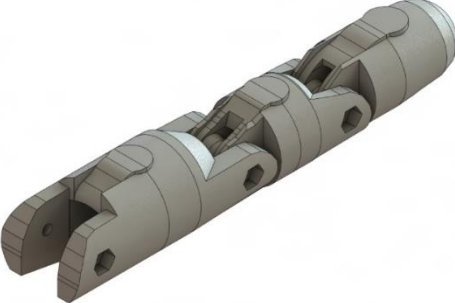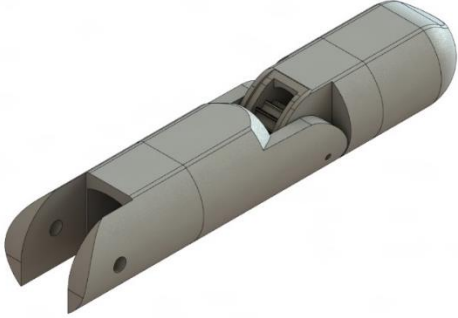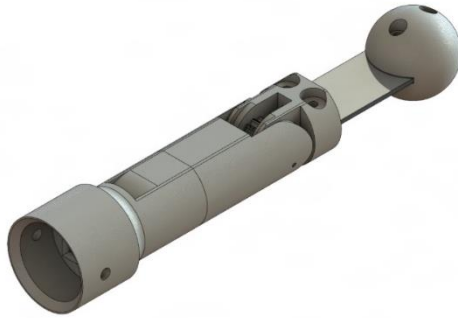
Figure 2.4 – Original InMoov Finger design using tendons and a servomotor

2. *Mechanical Design Iterations*

To improve on the original model, an iterative design process was followed: features and improvements were identified in consultation with the research team and especially the urologist; the improvements were implemented into a new revision; the revision was prototyped, tested, and analyzed; the prototyping results were discussed in team meetings; then new improvements were suggested to revise the model. Model changes sometimes required changes to other hardware components such as motors, force transmission methods (belts, gears), which also needed to be modeled and prototyped or purchased. Over the course of the research, multiple concepts, designs, and revisions (24 revisions) were proposed which were either rejected or further pursued. Some of the major revision milestones are presented and outlined in Table 2.1.

Table 2.1 – Some of the artificial finger revisions created during the design process

	Revision 1: • Original model as reverse-engineered from the InMoov STL files
	Revision 3: • Addition of mounting surfaces for a Force-Sensitive Resistor (FSR) • Addition of Countersinks to contain the bolt heads and nuts for patient comfort • Addition of a top bolt to easily remove the tip. • Addition of anchors inside to the tip to better mount the tendons

	Revision 6: • Conversion into a monolithic assembly to be prototyped on a 3D-printer with soluble support; no screws or pins are to be used as shafts • Softening of surfaces • FSR sensor can be mounted anywhere along the finger phalanges (flat surfaces)
	Revision 8: • Conversion into a single joint finger driven by a belt instead of tendons. • Addition of belt gear at the joint.
	Revision 13: • Use of strain gauge as the force sensor instead of a FSR. • Joint is enabled to rotate 90 degrees in either direction (up or down) • Addition of mounting bracket to mount the finger on a metallic extension tube
	Revision 16: • Use of a different geometry to deflect the strain gage sensor – a metal cantilever beam
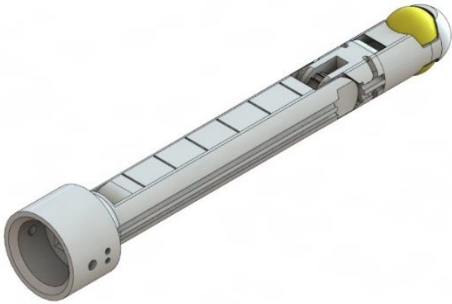
	Revision 20: • Reverting to a FSR sensor • Synthesis of a new tip with a contact hemisphere that presses on the sensor • Addition of wire routing channels • Addition of "hard stops" to limit joint rotation to 50 degrees. • Addition of gradations to identify insertion depth into the vagina

Table 2.1 – Some of the artificial finger revisions created during the design processTo

<u>Final Mechanical Design</u>

After multiple revisions, each requiring its own analysis, a final model was created, taking into account all the different improvements, limitations, and requirements learned during the iterative design process. The Smart Finger assembly includes the 3D-printed finger, the sensor, as well as the components needed for fastening and transmission of motion. The final assembly is shown in Figure 2.5.
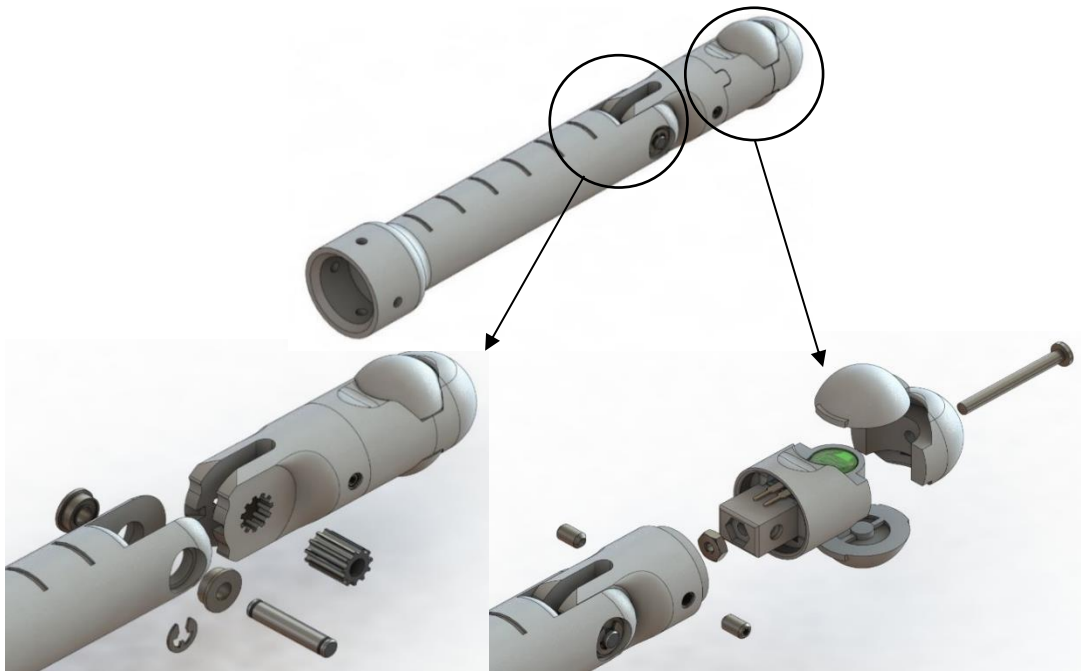
Figure 2.5 – The final model assembly of the Smart Finger

1. Replaceable tip

Since the finger is meant to be used by a physician, the assembly was required to be as user-friendly as possible. The fingertip which contained the sensor was designed to be easily removable and replaceable in cases of sensor maintenance and/or need for calibration. The tip is set into the finger using two socket set screws, which can be loosened to release the tip, see Figure 2.6.
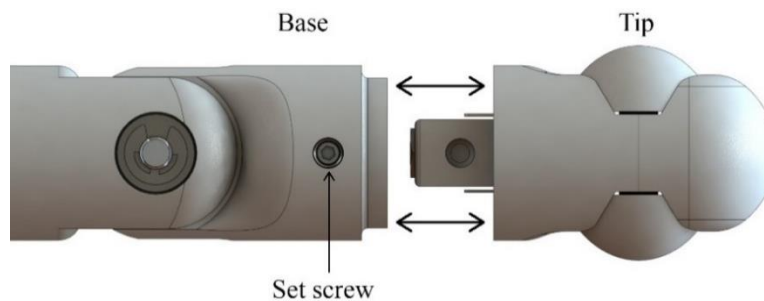
Figure 2.6 – Finger/Base assembly method. The tip is inserted into an opening within the base, and fixed using set screws.

The sensor establishes connection with the wiring to the main board using a spring-loaded contact, see Figure 2.7. This negates the need for soldering and de-soldering of the sensor each time the tip is removed from its base. It also makes the sensor independently replaceable in case of damage or wear. A third advantage to this design is the flexibility of implementing other types of sensors and fingertips in the future.
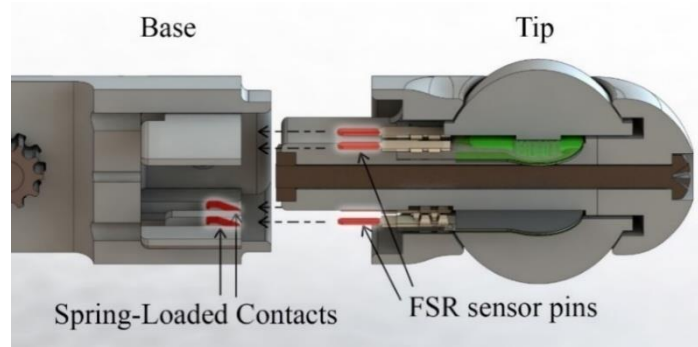
Figure 2.7 – The sensor circuit is completed using spring-loaded contacts in the base opening.

2. *Emergency hard-stop*

To prevent the finger from overly indenting the vaginal wall and exerting excessive force, an emergency mechanical hard-stop was added to the model interior as shown in Figure 2.8. The hard-stop prevents the joint from rotating more than 30 degrees, which is roughly the same angle at which a physician's actual finger is rotated to palpate the vaginal wall. This also successfully counters failure or misuse cases, such as when the actuator fails to stop, or when the user accidentally attempts to actuate the joint more than 30 degrees.
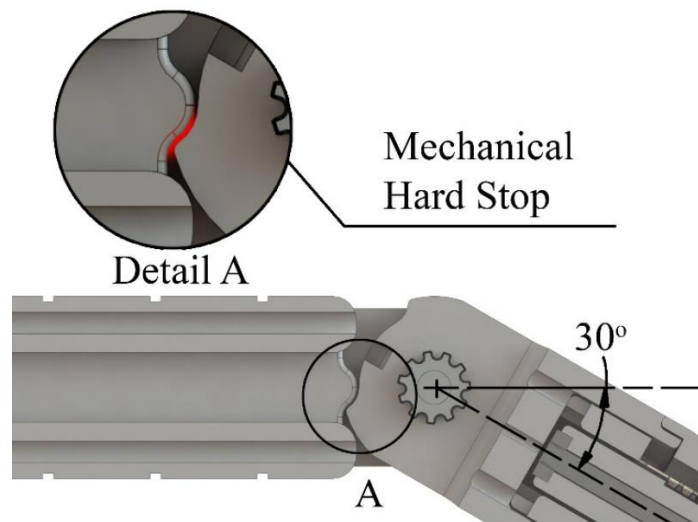
Figure 2.8 – The mechanical hard-stop. The joint geometry collides with a corresponding

protrusion within the stem to prevent further rotation of the joint.

3. Insert Depth Gradations

For consistency of measurement across different patients, the approximate insertion depth into the vagina needs to be the easily assessed. Gradations along the top of the finger can be used by the physician to define the insertion depth, see Figure 2.9. The distance from the center of the sensor to the first gradation is 5cm, while the distance between each two gradations is 1cm. In total, the finger can be inserted up to 10cm deep inside the vagina, which is slightly more than the average depth of the vagina in a normal state.
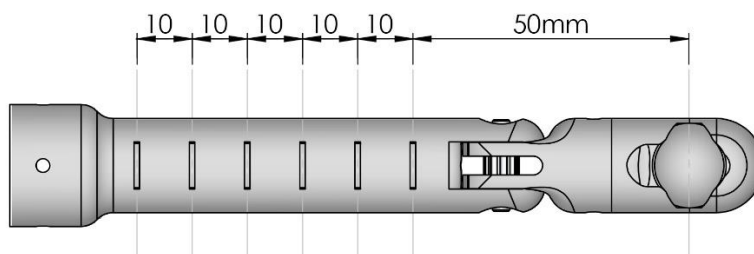
Figure 2.9 – Finger insertion gradations in mm

The Smart Finger can be fully covered using a plastic (Latex or other) cover/boot. This is due to the fact that no suction or direct contact is required between the sensing element and the vaginal tissue. Moreover, this feature is also possible because the sensor, its wires, and the power transmission method are all fully enclosed within the Smart Finger. A plastic cover eliminates the need for sterilization when the Smart Finger is to be used on a different patient, and reduces the risk for infection transmission.

Finite Element Analysis

In addition to functional specifications, medical devices have to be properly designed and analyzed for safety and failure analysis. Proper care must be taken to avoid injury to the patients. For this purpose, safety analysis has been conducted using machine design principles and finite

element analysis (FEA). The FEA was performed using ANSYS software with the analysis settings presented in Table 2.2. Note that if the material for the Smart finger changes then the analysis must be performed with the new material properties and the results re-analyzed.

Table 2.2 – Analysis settings and material properties used in FEA

Analysis Settings	
Analysis Type	Static Structural
Material Behavior	Linear Isotropic
ABS P400 Material Properties [26] [27]	
Tensile yield strength	14 MPa
Compressive yield strength	33 MPa
Young's modulus	1.6 Gpa
Poisson's ratio	3.6

Table 2.2To improve on the original model, an iterative design process was followed:

1. *Loading Conditions*

    There are 3 input loads on the assembly as shown in Figure 2.10:

    1. Fingertip Preload: the fingertip bolt and nut are tightened to preload the sensor.

    2. Belt Tension: the belt used for force transmission needs to be tensioned in order to maintain correct timing and prevent skipping.

    3. Reaction Force: the motor exerts a certain torque to actuate the fingertip which is countered by the reaction force from the vaginal tissue.
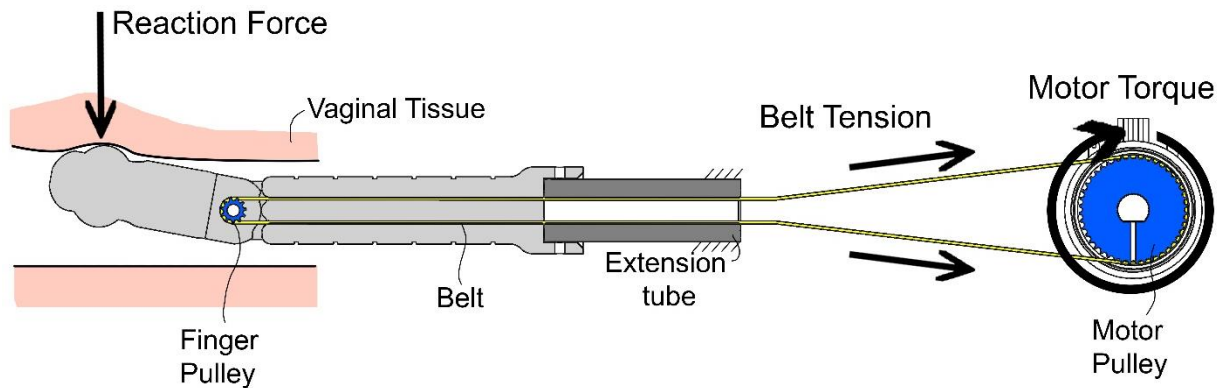
Figure 2.10 – Typical Loads acting on the assembly

Based on prior studies of soft tissue indentation, the reaction forces from indentation tests reach approximately 1.2N with 8mm to 10mm of indentation depth [7] - [13]. To reach the most conservative results, the following precautions were taken in the FEA:

- Typical reaction force: rounded up to 2N instead of 1.2N

- ABS yield strength: reduced to 60% of manufacturer's specifications to account for build orientation effects [26] [27], as will be discussed in Chapter 3.

- Strength analysis: performed on each part individually, instead of all the parts combined, by assuming that each part experiences the entire loading by itself.

- Mesh refinement loops: the mesh was refined at least once to check for stress singularities which can incorrectly appear as the true maximum stress point.

2. *Fingertip preload analysis*

As discussed in Chapter 3, the fingertip needs to be preloaded by tightening the bolt of the fingertip assembly, see Figure 2.11. Analysis using ANSYS was conducted on the fingertip components in isolation from the rest of the assembly. Symmetry was used to reduce computation time. The aim of the analysis was to assess the maximum preload which the fingertip can withstand before yielding or cracking. This would occur when the maximum equivalent Von-Mises stress,

24

σ_{max}, is equal to the material yield strength ($\sigma_y = 14\ MPa$). Therefore, different bolt adjustments were evaluated using ANSYS until the $\sigma_{max} = \sigma_y = 14 MPa$. The maximum fingertip preload was found to be 0.12mm which can be set using a micrometer or a Vernier caliper. The FEA setup and results are shown in Figure 2.12 and Figure 2.13, respectively.

A.   B.
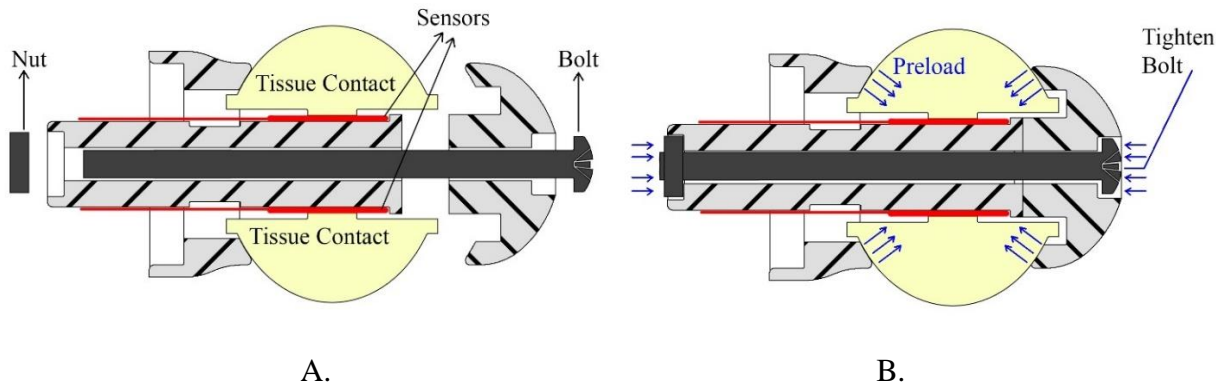
Figure 2.11 – A. The fingertip before sensor preload – B. The fingertip after sensor preload
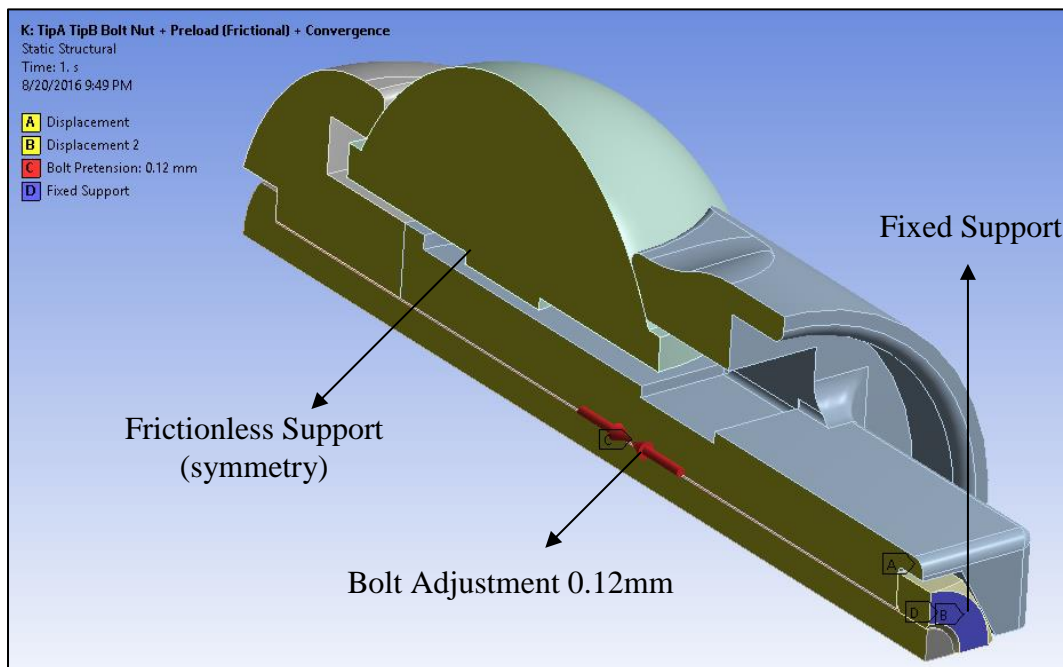
Figure 2.12 – FEA loading and support conditions for the fingertip preload analysis

$$\sigma_{max} = 14MPa$$
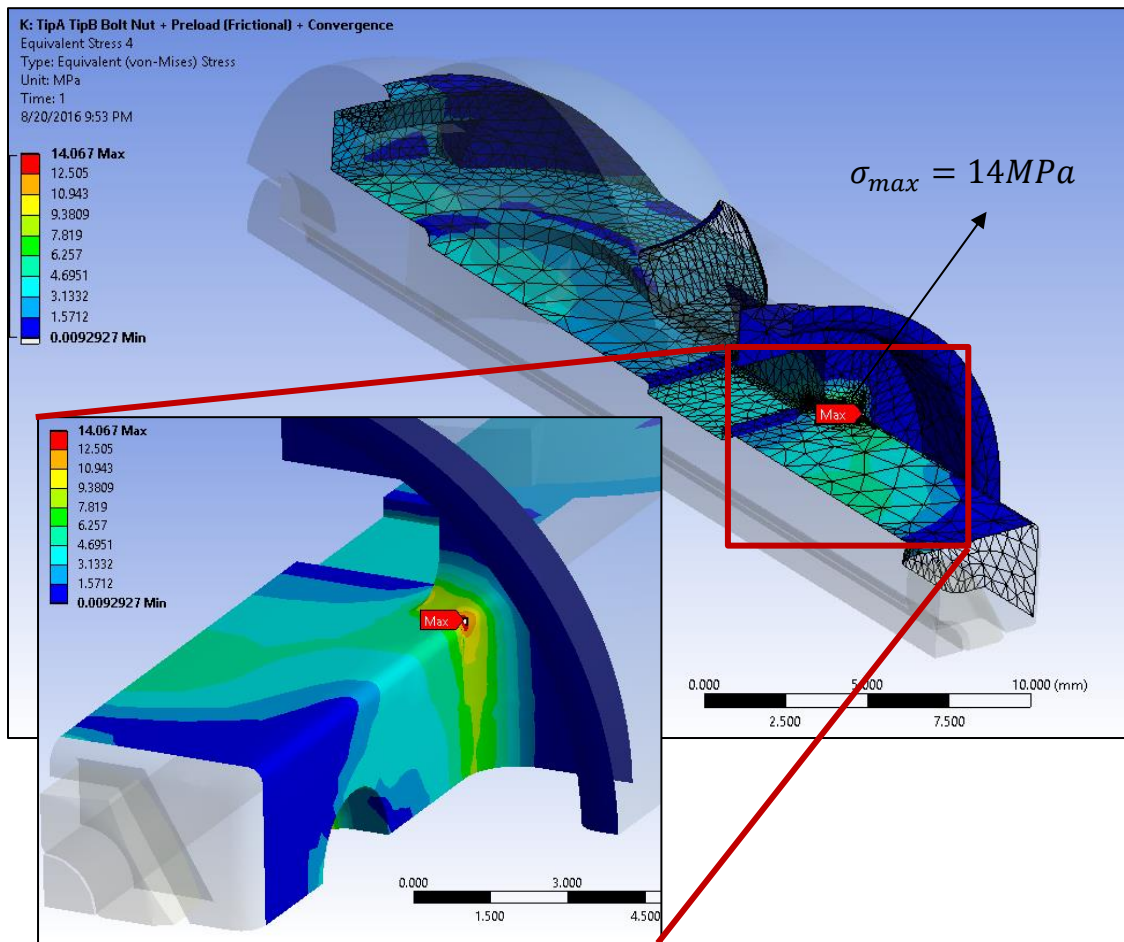
Figure 2.13 – Von-Mises Stress distribution due to the fingertip preload. Maximum Stress occurs at the location indicated "Max".

3. *Belt tension analysis*

To avoid slippage of the belt from the finger pulley and to maintain correct timing of the finger motion, the transmission belt needs to be tensioned as shown Figure 2.14. However, this tension applies stress onto the finger body. Analysis using ANSYS was performed to assess the maximum belt tension that can be applied without breaking the finger. Different tension forces

were considered in the analysis until $\sigma_{max} = \sigma_y = 14 MPa$. The analysis setup and results are shown in Figure 2.15 and Figure 2.16, respectively.
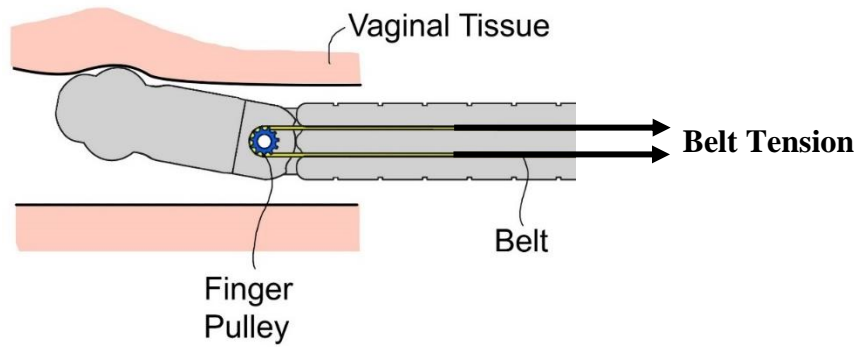
Figure 2.14 – The belt tension acts on the finger pulley, which in turn acts on the finger body
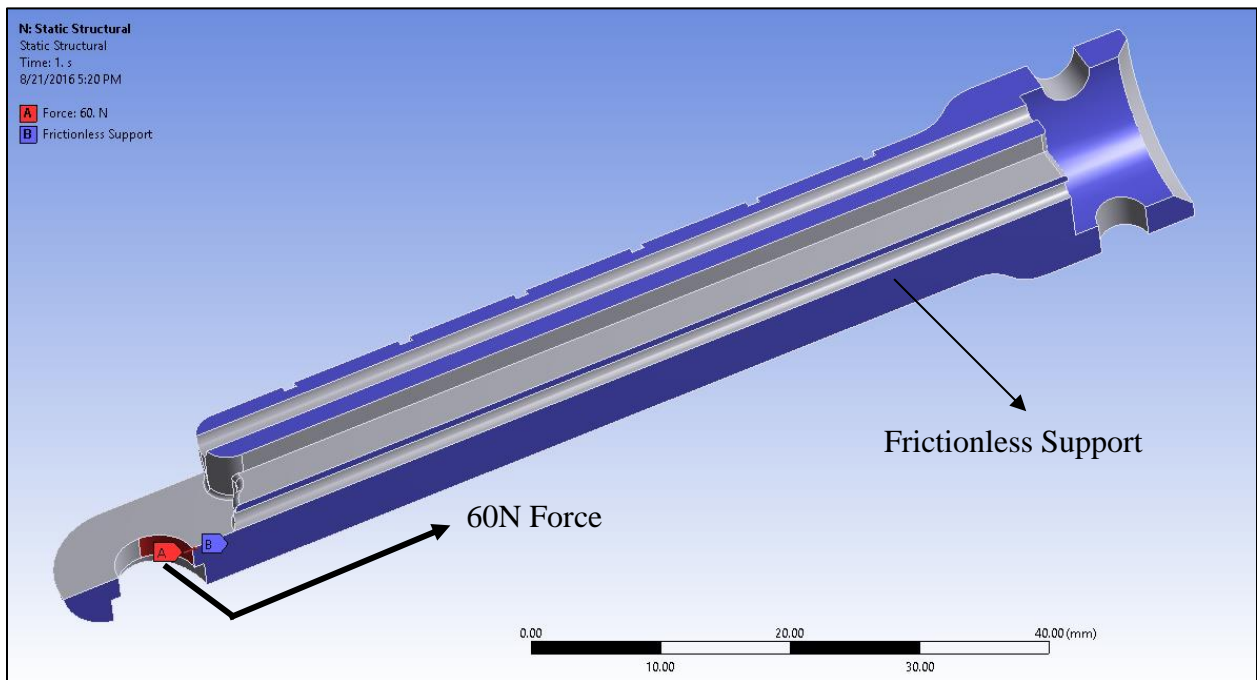
Figure 2.15 – FEA loading and support conditions for the belt tension analysis
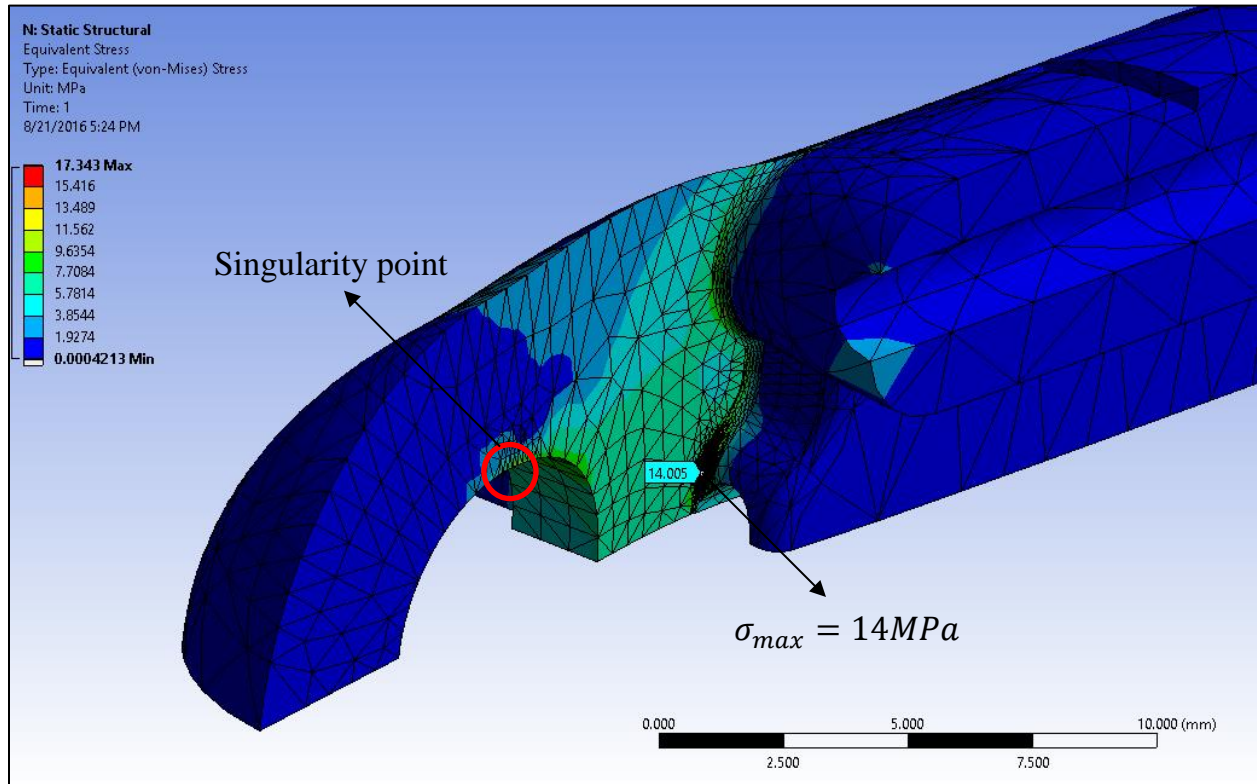
Figure 2.16 – Von Mises Stress distribution due to the belt tension

A singularity point was found at which the stress rises with mesh refinements and which was incorrectly shown as the maximum stress point, see Figure 2.16. By refining the mesh three times, the singularity was isolated. The maximum belt tension force was assessed to be 120N. Currently, there is no method developed to measure the applied belt tension; therefore, caution must be taken while tensioning the belt not to overload the finger. During device testing procedures, it was found that sufficient tensioning of the belt can be achieved without causing the finger to fail, which indicates that the required tensioning is below the 120N threshold.

4. *Reaction force analysis*

The principle of operation of the system requires a reaction force to be exerted on the sensors of the Smart Finger as shown in Figure 2.17. This reaction force affects the entire finger

assembly, but high stress points may arise in certain locations, such as the pulley teeth or the set screws. Again, analysis was performed on the parts where the highest stress is expected to occur. The maximum stress point was assessed to be 1.07 MPa at the gear teeth. Since the tensile yeild strength of ABS was defined to be 14MPa, the typical reaction force acting on the fingertip will not cause part failure. The analysis setup and results are shown Figure 2.18 and Figure 2.19, respectively.
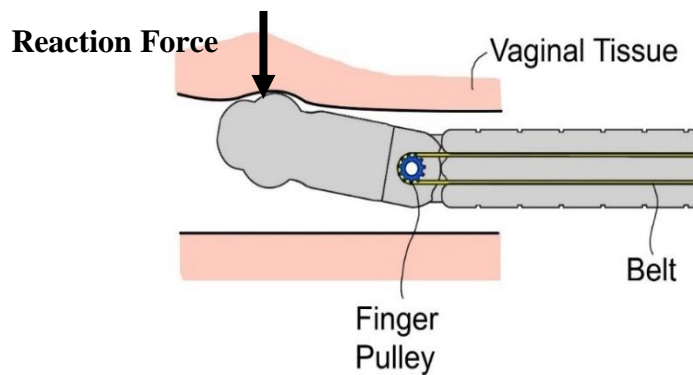
Figure 2.17 – The reaction force acts on the fingertip, and is subsequently transferred into the Smart Finger body
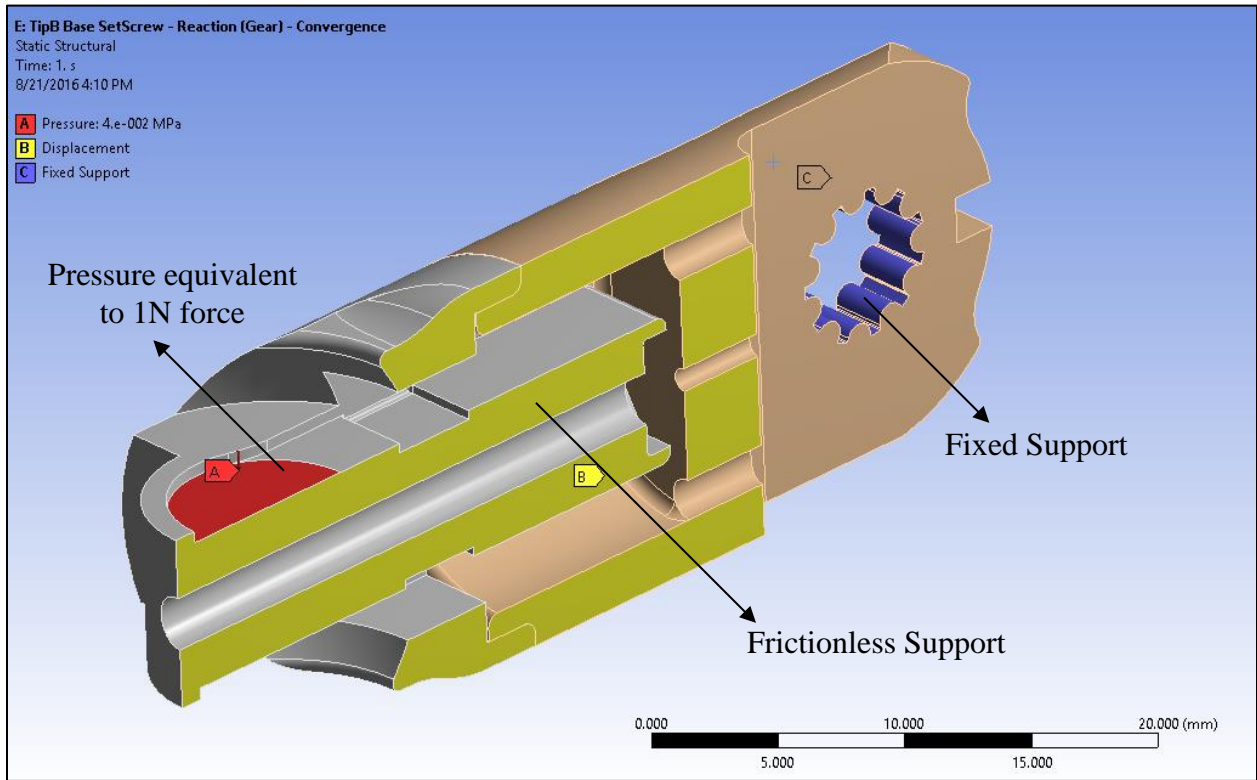
Figure 2.18 – FEA loading and support conditions for the reaction force analysis
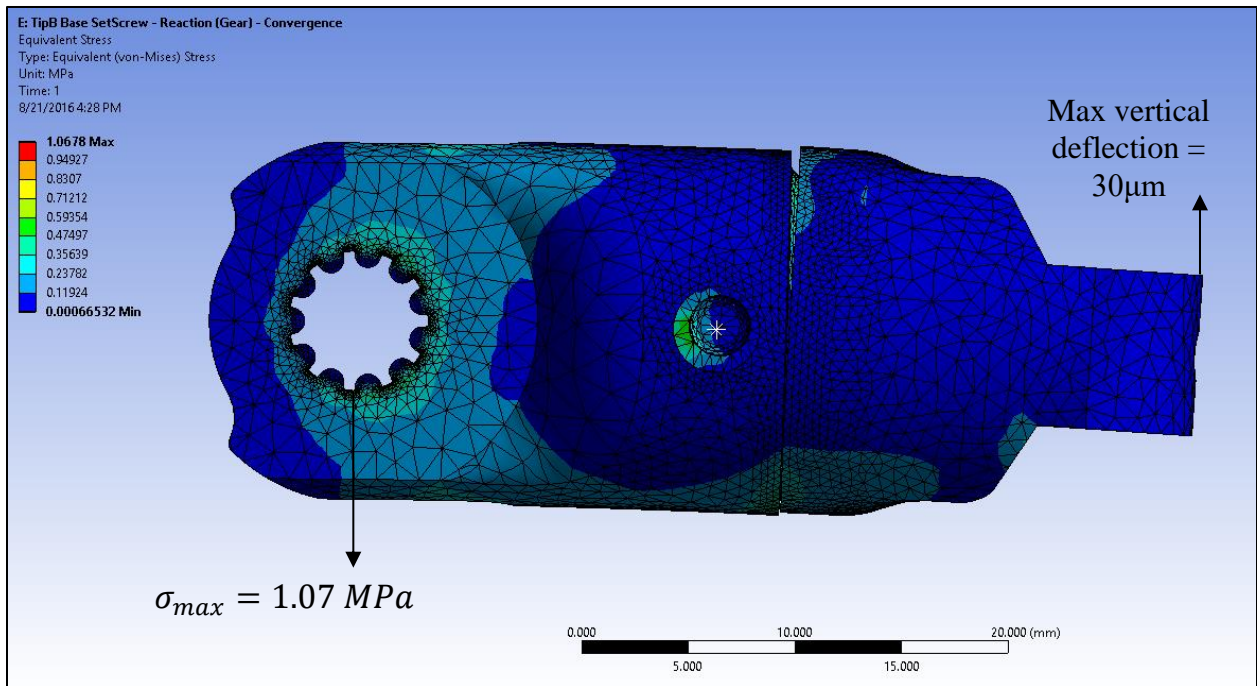
Figure 2.19 – Von Mises Stress distribution due to the reaction force

Chapter 3

SYSTEM PROTOTYPING

A complete prototype of the proposed system was fabricated for verification of operation and testing. Several components were designed and fabricated, such as the Smart Finger, the supporting structures, the electrical and electronic circuits, and the programming and GUI. All hardware equipment was mounted on a tripod for easy positioning during testing in the examination room and for transportation as shown in Figure 3.1.
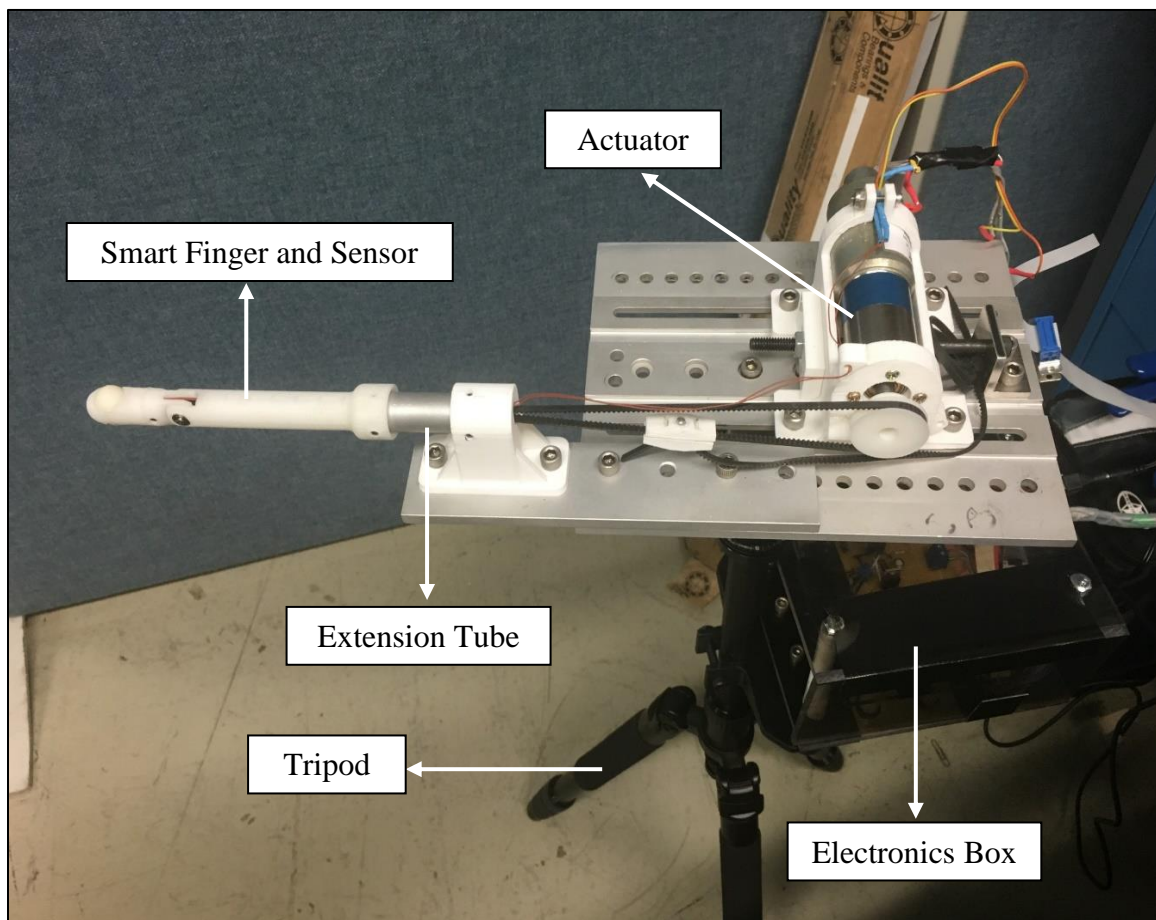
Figure 3.1 – All system hardware and electronics

The fabrication process used to prototype many parts of the system is Fused Deposition Modeling (FDM) – more commonly known as 3D-printing. This process provided an easy and quick method for prototyping, testing, and revising the design. Model and components revisions were 3D-printed at the UTA Manufacturing Automation and Robotic Systems (MARS) Lab using the Stratasys Dimension SST768 3D-printer. The 3D-printing material of choice is ABS, and slicing (printer path generation) was automatically performed by the Stratasys CatalystEX software. Revisions were tested using different soft materials such as rubber, foam, and skin to simulate the vaginal soft tissue. However, FDM suffers from a few caveats that require special considerations, which are discussed in Table 3.1 below. Some of the 3D-printed revisions are shown in Figure 3.3.

Table 3.1 – Limitations and considerations of FDM fabrication process

Limitation	Effects	Considerations
Layer Height	At best, the dimensional accuracy of the 3D-printed part can be as good as the height of each printed layer.	The layer height was set to its lowest value of 0.25mm (0.01in.) to minimize dimensional accuracy errors.
Bead/fiber width	Despite software considerations, the width of the bead/fiber increases outer dimensions over the nominal value design using CAD software. This especially affects part-to-part fits.	Through trial and error, clearances of 100μm (0.004 in) were assigned for tight fits, while 300μm (0.012in.) were assigned for loose fits.

Build Orientation and printing path	3D-printed parts are not completely solid. There is some separation between the layers and between individual fibers. The orientation of the separations is dependent on the build orientation and the extruder path, see Figure 3.2. This creates areas of stress concentration which affect part strength [26]- [28].	Parts were set to be printed in orientations that maximize strength. The build orientation was chosen to place fibers in the direction of critical loading. Areas of high stress concentration were also coated with a layer of a UV photopolymer to increase strength and toughness.

Table 3.1—*Continued*
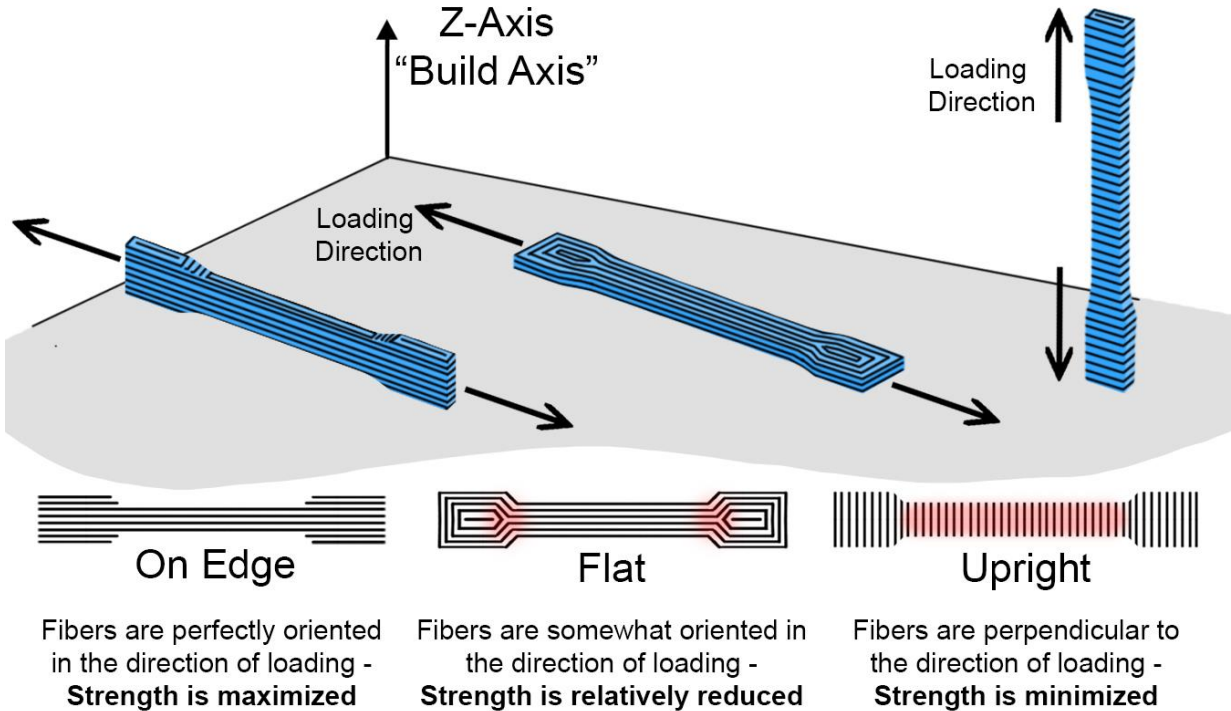
Figure 3.2 – Build orientation affects the strength of 3D-printed parts

Figure 3.3 – Some the prototyped revisions of the Smart Finger (oldest to newest, left to right)

Other load-bearing components such as the mounting base, the shaft of the Smart Finger joint, and the belt gear were fabricated in the UTA machine shop.

<div align="center">Force Sensor</div>

The force sensor of choice for the finger is the "Interlink Electronics FSR 400 Short" Force-sensitive Resistor, shown in Figure 3.4. The sensor is a polymer thick-film device that contains a conductive pattern. When the sensor is compressed, the resistance of the conductive pattern decreases relative to the compression force applied to it.

This sensor was chosen mainly for its low cost ($12 per unit), low profile (0.3mm thick), and ease of interfacing with the controller. However, it suffers some important limitations that need to be addressed in a future iterations of the device.

First, it has a non-linear logarithmic voltage output with the applied force. As the force increases, the voltage output increases, but also the slope of the output decreases with higher forces until it levels at a maximum voltage, see Figure 3.5. This can limit the working range to 300gr equivalent force, depending on the electric circuit used.
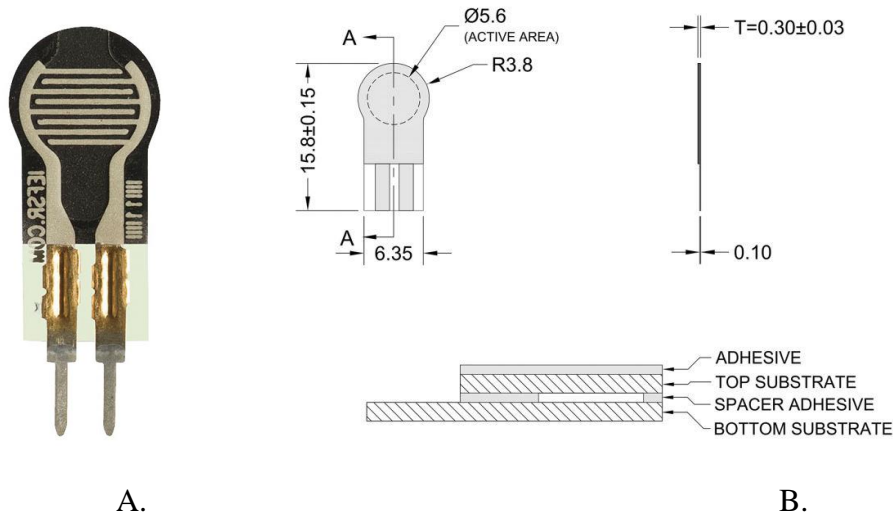
Figure 3.4 – A. Interlink Electronics FSR 400 Short – B. CAD drawing [29]

Second, it requires at least 50gr of equivalent force before generating a stable sensor output, which requires the user to preload the sensor before using it for measurements below that threshold; otherwise, the user risks operating in the "dead zone" where no force is being sensed.

Third, the repeatability of the sensor response is highly dependent on the repeatability of the sensor engagement method. As shown in Figure 3.4 B, the sensor active area is a circle of diameter 5.6mm. It was observed that the sensitivity of the sensor increases if the engagement surface pressing on the active area is somewhat smaller than the active area, rather than larger or equal to it. Thus, the engagement surface was designed to be 3.8mm in diameter. It was also observed that changes in the positioning or hardness of the sensor engagement surface causes changes in the sensor sensitivity. Therefore, a repeatable actuation method is needed to produce repeatable force measurements, which is discussed in the Sensor Engagement and Preload section.
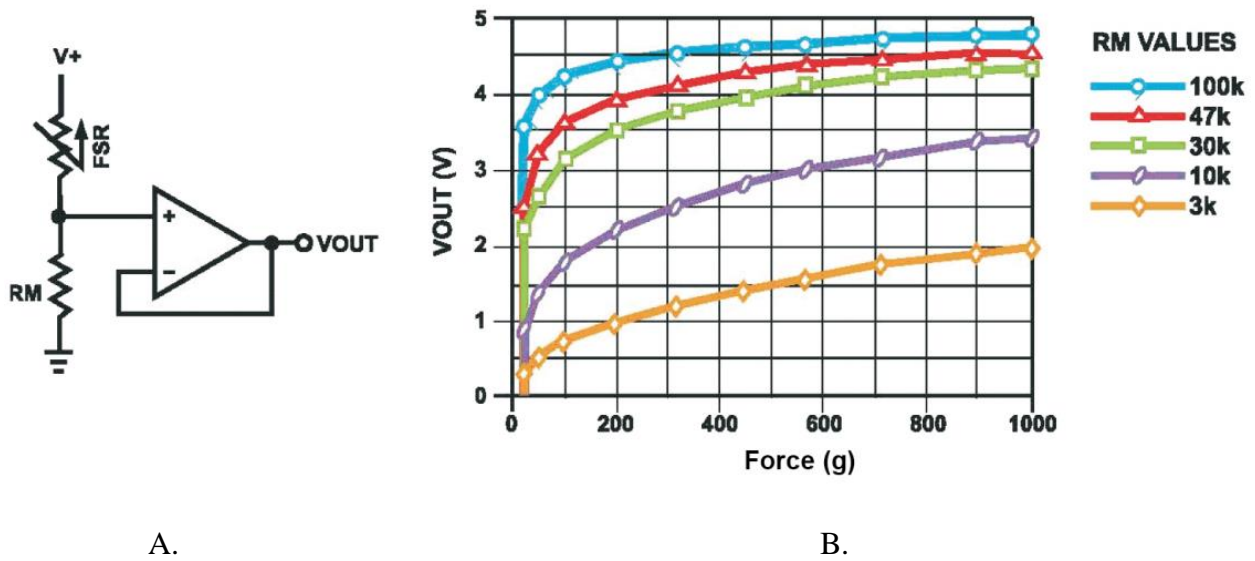
Figure 3.5 – A. Suggested FSR sensor integration circuit – B. Force versus Voltage output of the

FSR sensor as provided by the manufacturer [29]

1. *Sensor Engagement and Preload*

Since the repeatability of the FSR sensor is highly affected by the engagement

method/surface, a loading mechanism was designed to load the sensor in a consistent manner.

Additionally, the mechanism is also used to preload the sensor, due to the existence of the "dead

zone" between 0 and 50gr where the sensor output is either unstable or non-existent. The

mechanism consists of a hemisphere for tissue contact with a pressure button, housed inside the 2-

part fingertip, see Figure 3.6. The bolt presses the two parts of the fingertip together, which in turn

presses on the hemisphere, which in turn presses on the sensor to preload it, see Figure 3.7.
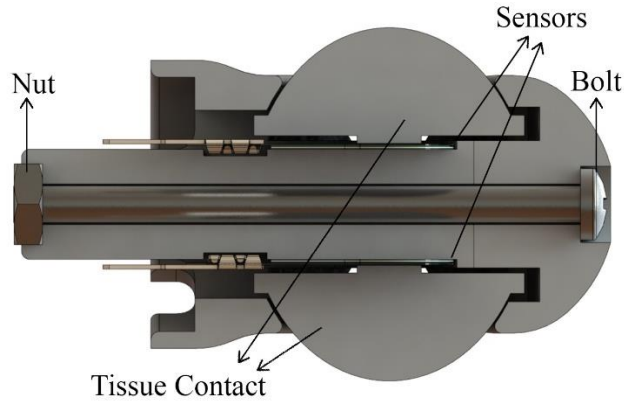
Figure 3.6 - Section view of the interior parts of the fingertip as normally assembled
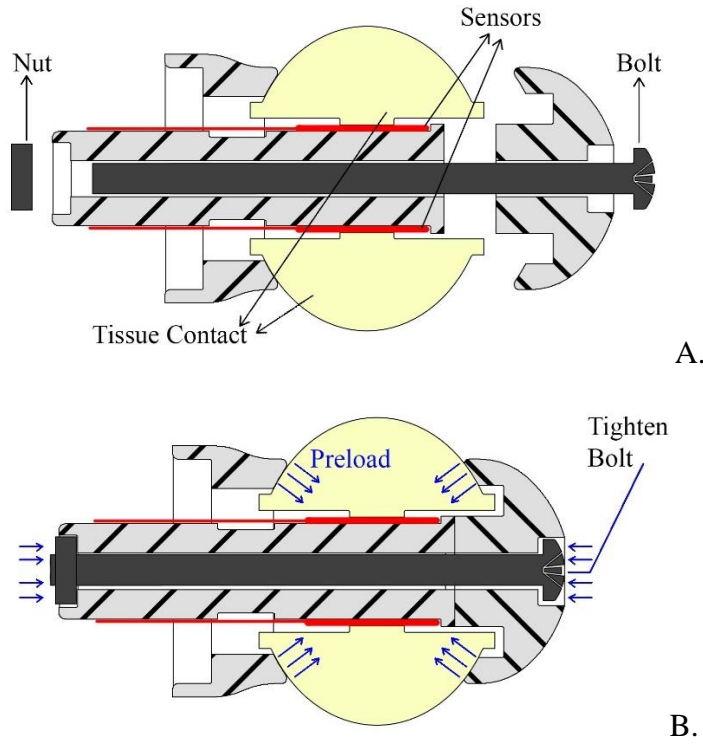
Figure 3.7 – A. The fingertip before sensor preload – B. The fingertip after sensor preload

It was observed that the output voltage response between 100gr and 300gr applied equivalent force can be assumed to be linear, which makes it the optimal range of operation for the sensor. Therefore, a preload exceeding 100gr is preferred.

2. *Sensor Characterization and Calibration*

The sensor output curves provided by the manufacturer are for demonstration purposes only due to the large variability in the response depending on the working conditions. Per the manufacturer integration guidelines, it is recommended to calibrate the sensor in its working environment. Hence, a calibration rig was designed to perform a static force calibration on the sensor using dead weights. The rig consists of a vertical carriage that holds dead weights, and fitted with a pressure plunger that presses on the tissue contact hemisphere, see Figure 3.8. The fingertip is attached onto the rig in the same way it is attached onto the Smart Finger.
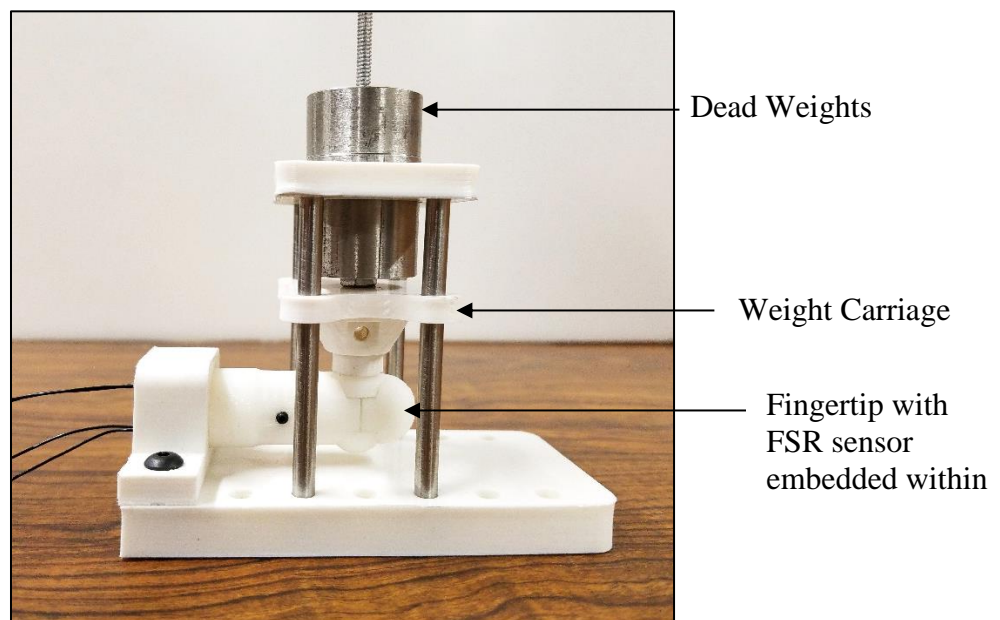
Figure 3.8 – Sensor calibration rig

The FSR sensor acts as variable resistor; its resistance R_{FSR} decreases logarithmically with the applied force. In order to measure this change in resistance, the sensor can be implemented in a voltage divider circuit with another known resistance R_M, see Figure 3.9. A known voltage V_s is applied to the circuit, and the voltage drop due to the resistance of the sensor is read.
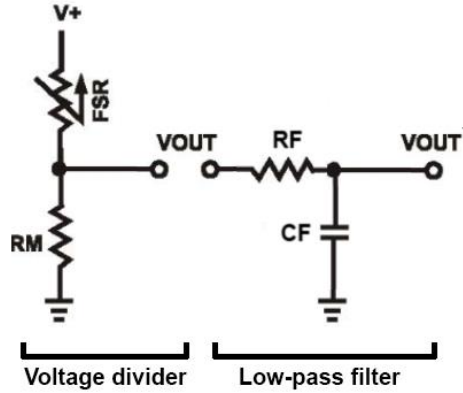
Figure 3.9 – Voltage divider circuit used to read the resistance change [29] and low-pass filter

circuit used to filter the signal noise

Additionally, a low-pass filter circuit was added to filter out any electrical noise in the

output signal. The filter circuit uses a 47 kΩ resistor and a 0.1µF capacitor to filter signal

frequencies higher than approximately 34 Hz.

$$V_{out} = \frac{R_M}{R_M + R_{FSR}} V_S \qquad \text{Equation 1}$$

$$V'_{out} = \frac{1}{1 + sR_F C_F} V_{out} \qquad \text{Equation 2}$$

According to Equation 1, the raw output voltage V_{out} is non-linearly proportional to the

FSR resistance, and the voltage response is affected by the complimentary resistance R_M. For a

complimentary resistance of 3kΩ and a supplied voltage of 5V, the produced calibration curve was

expected to be a logarithmic relation between the applied weight and the output voltage.

The calibration procedure was setup as follows. The sensor was tested using dead weights

ranging from 25gr to 300gr and discretized in steps of 25gr. This translates into 12 different weight

steps. Each weight step consisted of loading the carriage with the required weight and slowly

lowering it to press on the skin contact surface of the finger. Once it presses, a DAQ device was

used to record the voltage V'_{out} for 30 seconds to allow the signal to settle. Then, the carriage was

lifted and prepared for the next weight step. The time between each two steps was enough to allow the sensor to recover and release any residual stress.

The steps were not incrementally tested (as in 25gr, 50gr, 75gr, etc.), but rather randomized using an online randomizer in order to prevent any biasing in the response results. Overall, three runs of the complete 12 steps were performed, with the testing sequence randomized before each run. An example of test data produced for one of the three runs is shown in Figure 3.10.

A.   B.
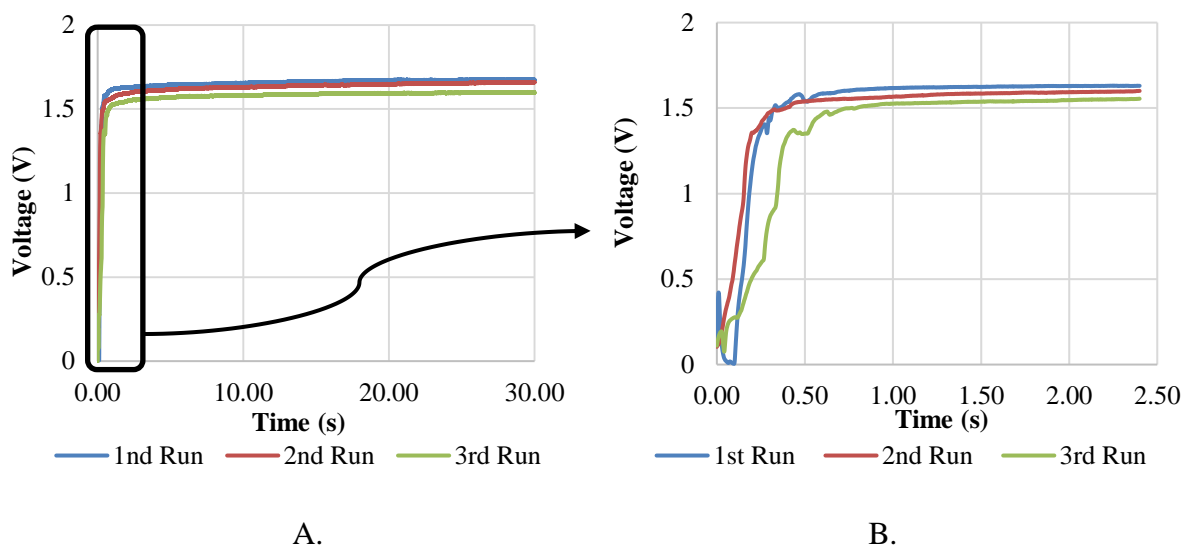
Figure 3.10 –Voltage versus Time test data for 200gr for A. (0-30 sec) and B. (0-2.5 sec)

It was observed that at an applied weight of 25gr, the sensor produced either no signal or an unstable signal. Therefore, the data set for an applied weight of 25gr was discarded. The sensor response to the step load appeared to match a first-order system response, with the voltage rising logarithmically and settling at a specific value after a certain time period. Therefore, to characterize the time domain characteristics of the sensor, the test data for each weight step was averaged and curve-fit on a first-order response, see.

A.   B.
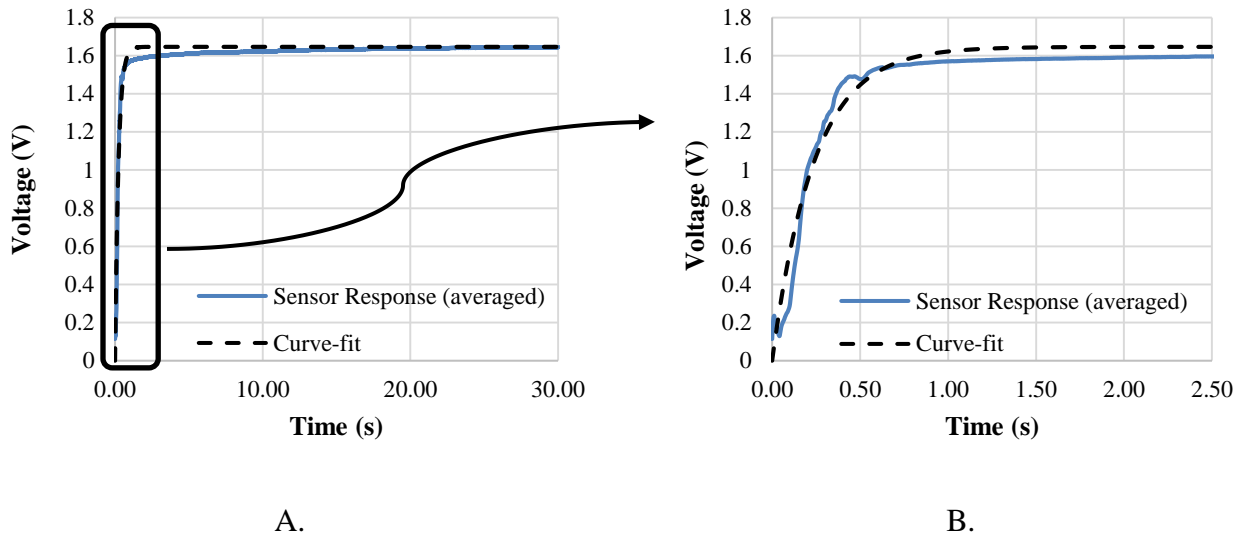
Figure 3.11 – Voltage response and curve-fit for 200gr for A. (0-30 sec) and B. (0-2.5 sec)

After testing was completed, the data was compiled and analyzed, see Figure 3.12, to produce the calibration equation, Equation 3. This equation is valid for an applied voltage $V_+ = 5V$, $R_M = 3K\Omega$, and weights between 50 gr to 300 gr.

$$Voltage = 0.6093ln(Weight) - 1.6593$$ Equation 3
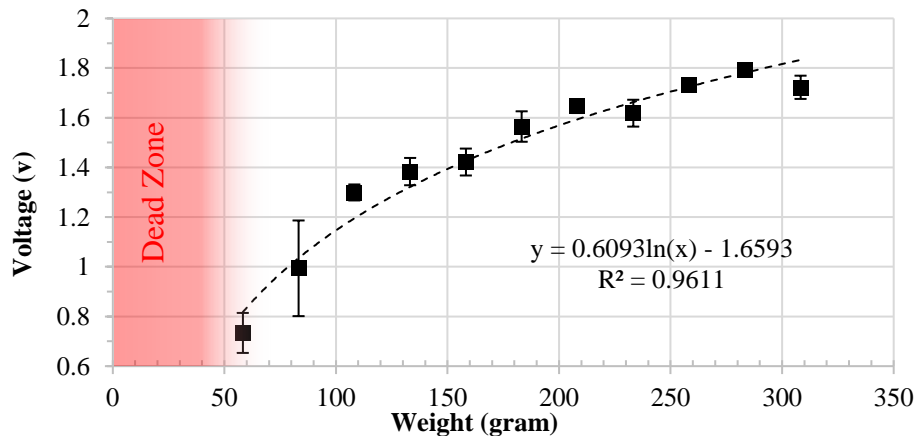
Figure 3.12 – Averaged calibration data points and calibration curve (dotted line)

The maximum deviation from the average reading was 15% and occurred on 75gr – likely due to the sensor sustaining some impact forces from the dead weight. The time constant of the

sensor response, τ, is defined as the time needed for the output voltage to reach 63.2% of its steady-state value. Assuming that the sensor steady-state value is the final value at $t = 30s$, the average time constant of the sensor response was approximately 0.21s. This corresponds to a settling time $T_s = 4\tau = 0.84s$.

Some important conclusions were drawn based on the calibration results. First, for the purposes of the system, the loading time of the vaginal tissue was expected to be between 0.5 and 3 seconds. A 0.84s settling time is somewhat higher than desired since the individual data points during the tissue loading period are used in the characterization procedure of the vaginal tissue. It is also important to note that at the applied weight of 25gr, the sensor produced either no signal or an unstable signal; this showed that the sensor possesses a "dead zone" for loads less than approximately 50gr. Another important realization from the calibration results is that the response of the sensor can be assumed to be linear between 100gr and 300gr, as seen Figure 3.13 and Equation 4.

$$Voltage\ =\ 0.0024 * Weight + 1.0768 \hspace{3cm} \text{Equation 4}$$
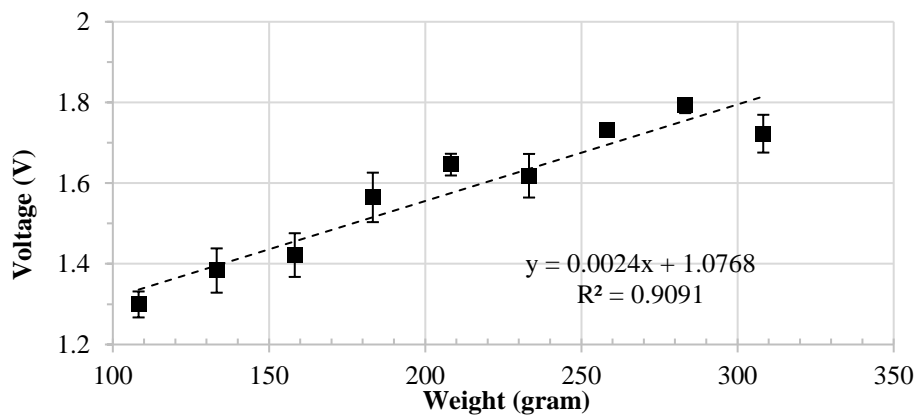
Figure 3.13 – Averaged calibration data points and calibration curve (dotted line) between 100gr and 300gr

Building on these findings, calibration was redone with an induced preload of 75gr on the sensor to surpass the dead zone" between zero and 50gr. The calibration procedure with the preload was different than the initial calibration with no preload on the sensor. The applied loads were not randomly-ordered, but rather increased and then decreased incrementally. The reason for this calibration procedure change is to attempt to recreate the increasing force on the sensor as it presses on the soft tissue then the decreasing force as the tissue relaxes. It was found that each time the load was removed, the sensor baseline voltage increased rather than remaining constant, see Figure 3.14. Additionally, between each two identical load steps (loading and unloading), there was an increase in the reading of up to 10% of full-scale. It was concluded that the sensor retains some of the applied load due to its inability to fully recover.
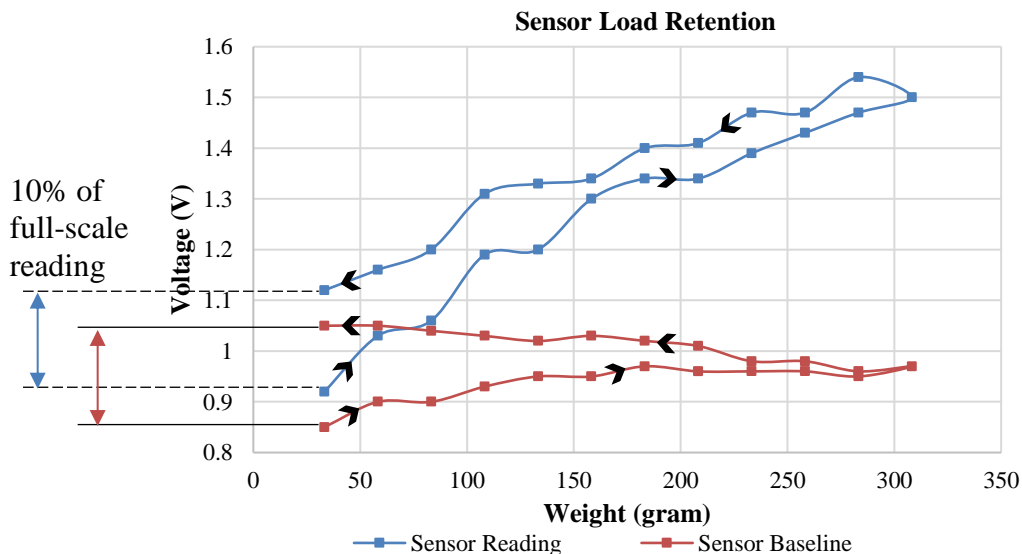
Figure 3.14 – Sensor reading and baseline with 75gr preload

The sensor characterization revealed the limitations and weaknesses of the FSR sensor – which were not clearly apparent at the time of purchase. Without any preload on the sensor, a "dead zone" exists between 0 and 50gr where no load is read; additionally, the sensor settling time

was found to be within the range of the expected loading time ($T_{settling} = 0.84s$ compared to $T_{loading} = 0.5s \ to \ 3s$). With preload on the sensor, the sensor is unable to recover when unloaded and the sensor readings will become inaccurate with usage. It was concluded that the FSR sensor may sufficiently work as a proof-of-concept, however a more specialized and more reliable sensor (e.g. load cell, piezoresistive, etc.) should be used for measuring the tissue reaction forces. Chapter 5, "CONCLUSIONS AND RECOMMENDATIONS", will further discuss recommendations for improvements to the sensor and future plans.

Actuator and Power Transmission

For actuation and power transmission, the final design uses a DC-motor along with a timing belt for power transmission. Initially, a servo motor was used to actuate the finger. However, the servo motor suffered from a few important limitations. First, the servo motor has repeatability issues under load, with the position error of the motor being about ±8 degrees. Second, since the servo control circuit is embedded within the motor, a feedback signal to verify the current position could not be acquired. These limitations were addressed by using a high-end DC-motor/encoder combination. The motor can be driven using pulse width modulation (PWM) to position within the needed motor angle, and the encoder feedback can be read to control the position. The motor of choice was the Faulhaber 3557CS with a gearbox and encoder [30]. Its high stall torque (1.6 Nm) and high no-load speed (128 rpm) are well above the working requirements of the system.
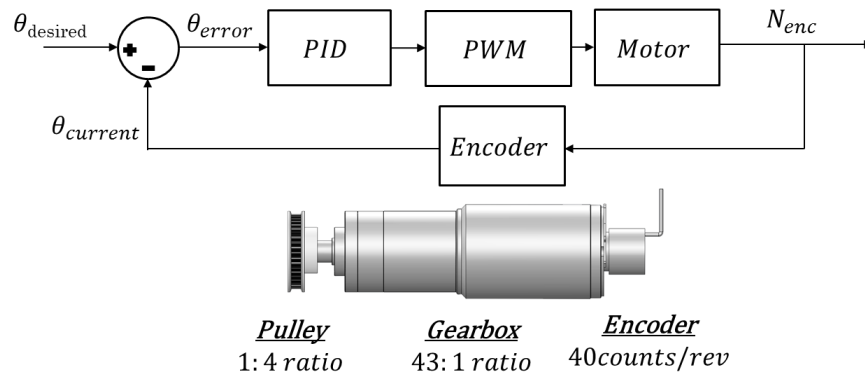
Figure 3.15 – Control loop of the DC-motor

The angular positioning of the motor was controlled using PID control. The PID gains were selected to prevent overshoot and minimize steady state error. The desired motor angle is set by the user, while the current motor angle is read by the attached encoder. The error between the desired and the current angle is fed into the PID controller, and the controller output is converted into a PWM signal that is used to drive the motor. For power transmission to the finger joint, a timing belt is used with a 1:4 ratio (1 motor rotation = 4 finger joint rotations).

As explained in the SYSTEM DESIGN chapter, the actuator applies a given displacement profile on the soft tissue via the Smart Finger. This displacement profile corresponds to a certain actuation profile for the actuator. The actuation profile of the motor consists of three actions, shown in Figure 3.16:

- Ramp Upward (tissue loading) for a time duration t_u between 0.5s and 3s

- Hold (tissue relaxation) for a time duration t_h between 1s and 10s

- Ramp Downward (tissue unloading) for a time duration t_d between 0.5s and 3s
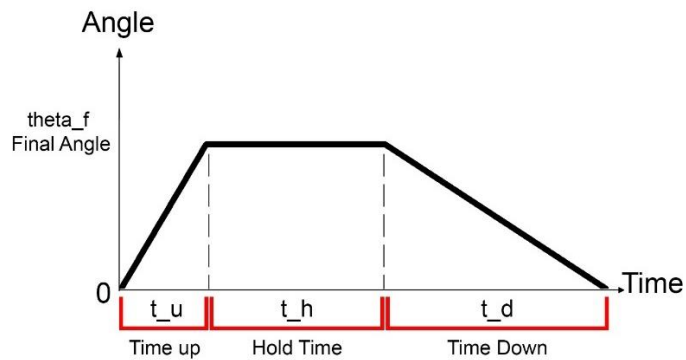
Figure 3.16 – Motor actuation profile

The actuation profile is parametrized by the different durations (t_u, t_h, t_d) and the final angle θ_f. The administering physician is able to define these parameters as desired using the Graphical User interface (GUI). During t_u, the tissue is being indented by the finger; during t_h the tissue is being held at a fixed strain level; during t_d the tissue is being released by retracting the finger.

Controller and GUI

The controller of choice is a National Instruments (NI) myRIO controller. It is an embedded hardware development tool that can be used to interface sensors, actuators, and other hardware. It was programmed using NI's LabVIEW software. LabVIEW was also used to create a Graphical User Interface (GUI) so that the user can interact with the Smart Finger. The GUI was programmed by Christopher E. Abrego, a research collaborator and a doctoral student at the MARS lab at University of Texas at Arlington. The GUI provides multiple control capabilities for the user such as controlling the actuator manually or through automatic motion; assigning the motor profile of motion; inputting the test date, number, and patient name. The GUI also displays the waveform of the sensor signal to the user in real-time.

The steps to be followed in order to conduct a test via the GUI are as follows:

1. Specify the upward, hold, and downward motion durations and angles, see Figure 3.17.
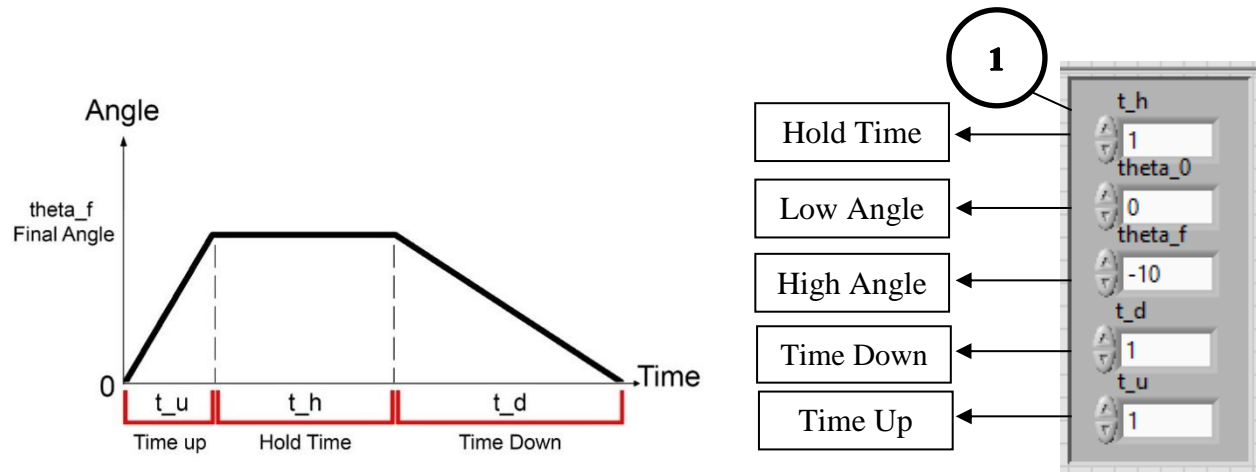
Figure 3.17 – Motor actuation profile (left) and GUI settings for motor actuation profile (right)

2. Switch to automatic testing, and enter the test number and the patient information, see Figure 3.18.

3. Click "Begin Motion". When the motor is powered, the "MotorOn" light will illuminate, see Figure 3.18.
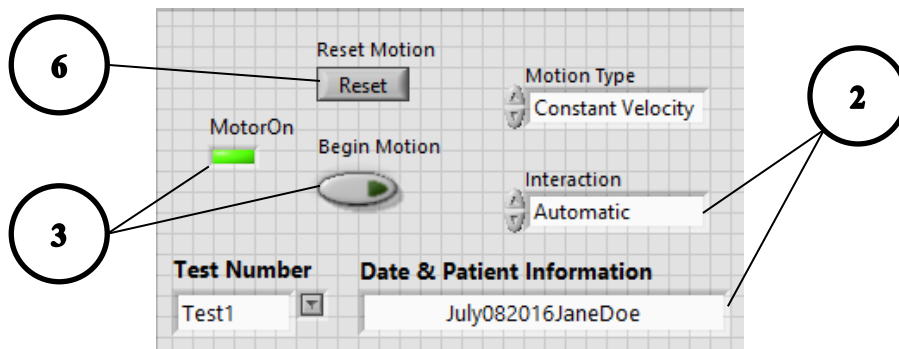
Figure 3.18 – Test Information and Test Start settings

4. As the motor is rotating the Smart Finger joint, the user can observe the real-time sensor signal via the waveform graph, see Figure 3.19.

5. When a test is in progress, the "TESTING" light will illuminate in RED to inform the user to wait until the current test is complete before conducting another test, see Figure 3.19.
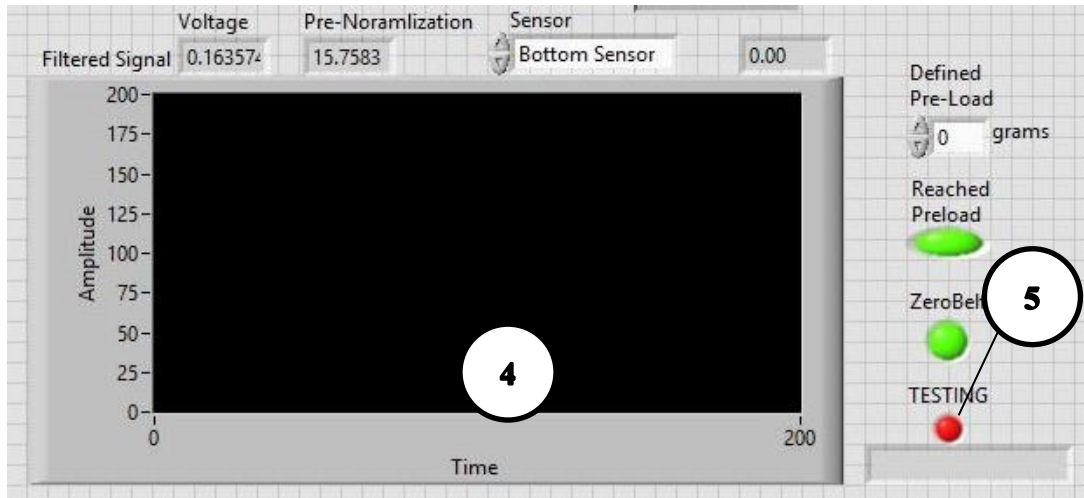
Figure 3.19 – Sensor Signal Waveform and test indicator lights

6. To conduct another test, the operator can change the test number and/or the patient information and press "Reset Motion", see Figure 3.18.
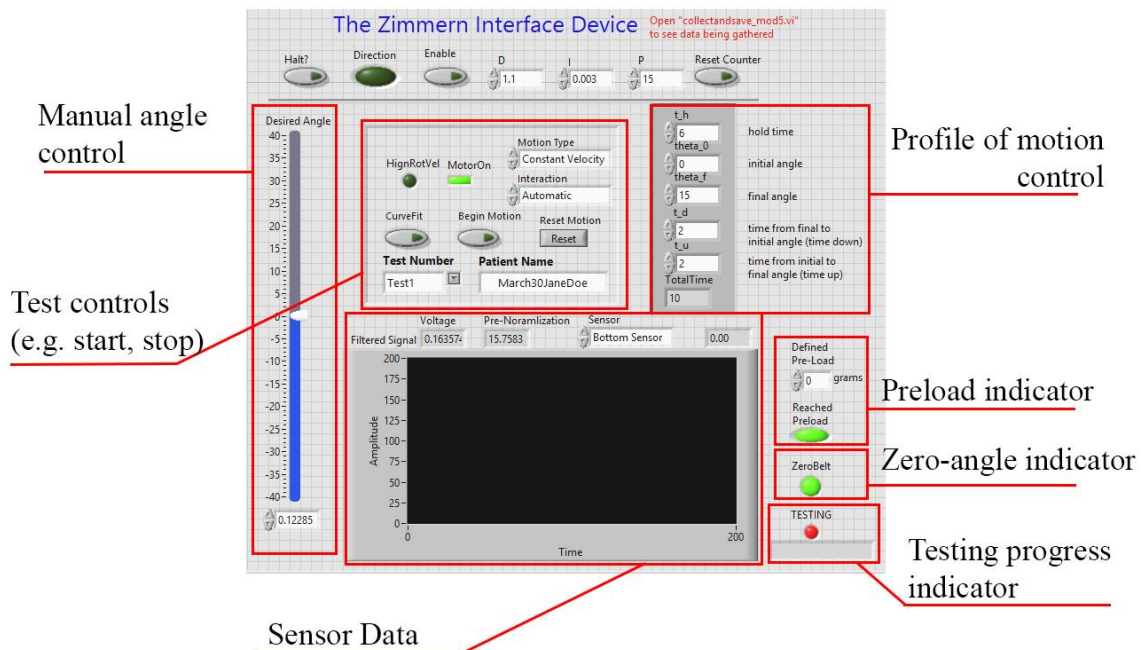
Figure 3.20 – Complete front panel of the graphical User Interface

Chapter 4

SYSTEM TESTING

The main objective of this research was to create an automated device, which can be used to characterize the biomechanical properties of soft tissue in-vivo. The developed system prototype was tested on six patients between July 26th and 28th 2016. The tests were conducted with the consent of the patients and administered by a urologist in the University of Texas Southwestern Medical Center, see Figure 4.1. The automatic curve-fitting of the test data was not employed in real-time during these tests due to limitations of the sensor and the need for further fine-tuning of the software (at the time of testing). Therefore, manual analysis of the data was to be conducted in the University of Texas at Arlington after the data was collected.

Figure 4.1 – In-Vivo testing environment of the system

Viscoelastic Modeling

The literature survey conducted on viscoelastic modeling of human soft tissue has shown that biological soft tissue behaves as a non-linear viscoelastic solid. A viscoelastic material is one

that exhibits stress relaxation, creep, and hysteresis, and viscous behavior causes a time-dependent response in the material upon loading. Linearity is concerned with the dependence or independence of the response on the response time history. In other words, if the material properties change as the material is subjected to a certain stress or strain, the material is considered non-linear.

A literature survey of more than 25 papers concluded that there are 2 main approaches for modeling viscoelastic behavior of soft tissue. First, the differential model which uses analogous mechanical elements such as springs and dashpots, and results in a model equation that is typically a differential equation of first or second order. Examples are the Maxwell model, the Kelvin-Voight model, and the Standard Linear Solid (SLS) model. The second model is the integral model which uses integro-differential equation to model the viscoelastic behavior. For example, the Boltzmann Superposition Model and Fung's Quasilinear Viscoelastic Model are integro-differential models.

The literature survey has also shown that there is no strong consensus around a preferred model for soft tissue modeling. Studies are often conducted with the sole purpose of designing more accurate models of soft tissue behavior. Therefore, the research outlined in this document used the most basic models as a starting point for comparison with the test data acquired from the patients. More in-depth research into the most accurate models is needed once a larger and more reliable set of data is obtained.

1. Maxwell Model

The Maxwell model is the simplest viscoelastic model that can be used to curve-fit a force response due to a given displacement (or indentation). The Maxwell model is a linear differential

model that uses a spring and dashpot in series to include both the elastic and viscous portions of

the response, see Figure 4.2.
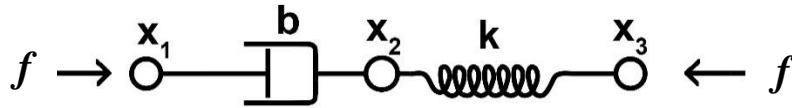
Figure 4.2 – The Maxwell Model

When the model is subjected to a certain force f, both the spring and dashpot produce a

corresponding reaction force. The reaction force of the spring is directly proportional to the

displacement x, while that of the dashpot is proportional to the displacement rate dx/dt. The

proportionality factors of the spring and dashpot are called the spring constant, k, and the damping

coefficient, b, respectively, which are assumed to be fixed in this research.

Since both the spring and dashpot are subjected to the same force $f(t)$, then

$$f(t) = k[x_2(t) - x_3(t)]$$ Equation 5

$$f(t) = b\frac{d}{dt}[x_1(t) - x_2(t)]$$ Equation 6

Since the total deformation $u(t) = x_1 - x_3 = (x_1 - x_2) + (x_2 - x_3)$, then

$$\frac{d}{dt}u(t) = \frac{d}{dt}(x_1 - x_2) + \frac{d}{dt}(x_2 - x_3)$$ Equation 7

$$\frac{d}{dt}u(t) = \frac{1}{k}\frac{d}{dt}f(t) + \frac{1}{b}f(t)$$ Equation 8

$$\left(\frac{b}{k}D + 1\right)f = b \cdot Du$$ Equation 9

where D is the differential operator $D = d/dt$.

Then, the force response is a first order differential equation with the displacement $u(t)$

as an input or a forcing function. Consequently, the actual force response is both dependent on

51

time and on the input displacement. The response for a ramp input or a step input could be predicted as follows.

For a step input $u(t) = u_o$, Equation 9 becomes

$$\left(\frac{k}{b}D + 1\right)f = 0 \qquad\qquad \text{Equation 10}$$

Then, solving the differential equation by assuming zero initial conditions, the force response is in the form

$$f(t) = ku_o \exp\left(-\frac{k}{b}t\right) \qquad\qquad \text{Equation 11}$$

For a ramp input $u(t) = vt$, Equation 6 becomes

$$\left(\frac{k}{b}D + 1\right)f = bv \qquad\qquad \text{Equation 12}$$

Then, solving the differential equation by assuming zero initial conditions, the force response is in the form

$$f(t) = bv\left[1 - \exp\left(-\frac{k}{b}t\right)\right] \qquad\qquad \text{Equation 13}$$

Figure 4.3 – Maxwell model force response due to A. Step input, B. Ramp input

The force relaxation response of a Maxwell model is characterized by the complete dissipation of the force – where the force due to a step displacement goes to zero at final time as shown in Figure 4.3 A. From Equations 11 and 13, the characteristic parameter for a 1st order system, such as the Maxwell model, is the time constant $\tau = \frac{b}{k}$. This parameter can be used to characterize the behavior of the vaginal tissue by curve-fitting the force response to Equations 11 and 13.

2. *Standard Linear Solid (SLS) Model*

A better suited model for this research is the Standard Linear Solid (SLS) model. Whereas the Maxwell model is unable to model creep behavior, the SLS model can be used to model both creep and stress relaxation behavior for many viscoelastic materials. Additionally, the SLS model force relaxation response is not characterized by complete dissipation of the force. Some residual amount of force is conserved in the system at the final time. Therefore, as the name suggests, the Standard Linear Solid model is more suitable for modeling linear viscoelastic solids.

The SLS model consists of a Maxwell model (spring and dashpot in series) parallel with a spring. The spring rate of the series spring is k_s while that of the parallel spring is k_p, and the damping coefficient of the dashpot is b, which are assumed to be fixed in this research.
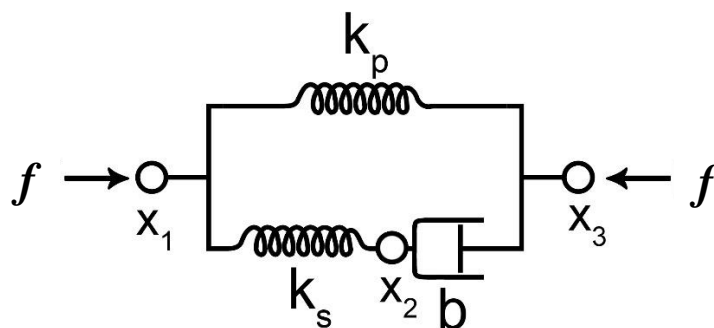
Figure 4.4 – The Standard Linear Solid Model

Let $u(t) = x_3 - x_1$ as the total displacement acting on the model, let $u_s = x_3 - x_2$ as the displacement acting on the Maxwell spring, and let $u_d = x_2 - x_1$ as the displacement acting on the Maxwell damper. Therefore,

$$u(t) = u_s(t) + u_d(t) \qquad \text{Equation 14}$$

From the previous subsection, the two components of the Maxwell model are subjected to the same force, $f_s = f_d$

$$k_s u_s(t) = b \frac{d}{dt} u_d(t) \qquad \text{Equation 15}$$

rearranging yields,

$$\frac{d}{dt} u_d(t) = \frac{k_s}{b} u_s(t) \qquad \text{Equation 16}$$

The total force acting on the system is equal to the sum of the forces acting on each leg; where the force acting on the parallel spring is f_p and the force acting on the Maxwell leg is f_s

$$f(t) = f_p + f_s = k_p u(t) + k_s u_s(t) \qquad \text{Equation 17}$$

rearranging yields,

$$u_s(t) = \frac{1}{k_s} f(t) - \frac{k_p}{k_s} u(t) \qquad \text{Equation 18}$$

Taking the time derivative of Equation 14 and substituting Equations 16 and 18,

$$\frac{d}{dt} u(t) = \frac{d}{dt} u_s(t) + \frac{d}{dt} u_d(t)$$

$$\frac{d}{dt} u(t) = \frac{1}{k_s} \frac{d}{dt} f(t) - \frac{k_p}{k_s} \frac{d}{dt} u(t) + \frac{1}{b} f(t) - \frac{k_p}{b} u(t) \qquad \text{Equation 19}$$

rearranging yields,

$$\left(\frac{b}{k_s} D + 1 \right) f(t) = \left[\left(b + \frac{bk_p}{k_s} \right) D + k_p \right] u(t)$$
$$(\tau_f D + 1) f(t) = (\tau_u D + 1) k_p u(t)$$

Equation 20

54

where $\tau_f = \dfrac{b}{k_s}$ and $\tau_u = \dfrac{b}{k_s} + \dfrac{b}{k_p}$.

Similar to the Maxwell model, the force response of the SLS model, Equation 20, can be described as a first order linear differential equation with the displacement $u(t)$ as an input or a forcing function. The actual force response is both dependent on time and on the input displacement.

For a step input $u(t) = u_o$, solving the differential equation with zero initial conditions, the force response is

$$f(t) = k_p u_o \left[1 - (1 - \tfrac{\tau_u}{\tau_f}) \exp\left(-\tfrac{t}{\tau_f}\right)\right]$$

Equation 21

For a ramp input $u(t) = vt$, solving the differential equation with zero initial conditions, the force response is

$$f(t) = k_p v \left[t + (\tau_u - \tau_f)\left(1 - \exp\left(-\tfrac{t}{\tau_f}\right)\right)\right]$$

Equation 22

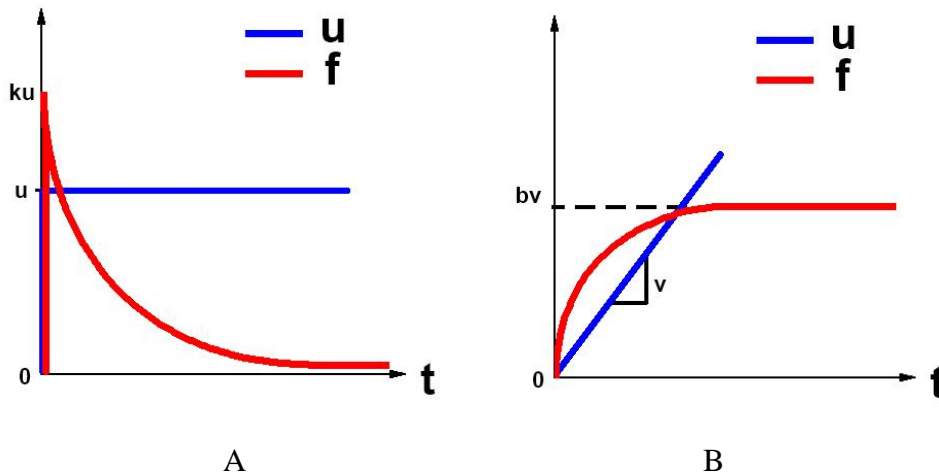A.   B.
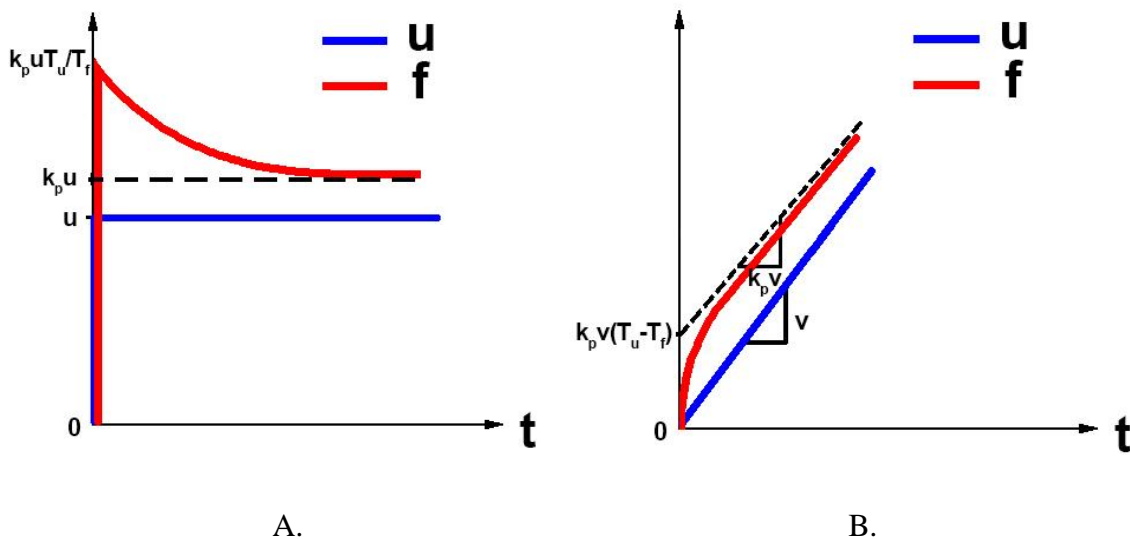
Figure 4.5 – SLS model force response to A. Step input, B. Ramp input

The force relaxation response of the SLS model is characterized by a partial dissipation of the force, which is more suitable for a viscoelastic solid, see Figure 4.5. Similar to the Maxwell model, it is apparent from Equations 21 and 22 that the characteristic parameter is the time constant $\tau_f = \frac{b}{k}$ associated with the exponential decay. Therefore, whichever of the two models is to be used, the exponential time constant can be used to characterize the response of the system.

3. *Quasilinear viscoelastic (QLV) model*

Another model used to model soft tissue behavior and presented in this document for completeness is an integro-differential model called the Quasilinear Viscoelastic (QLV) Model. A literature survey of 25 papers modeling soft tissue as viscoelastic material concluded thatthe QLV Model was used in ten papers more than any other model [9] [31-39]. The QLV model was proposed by Fung in 1972 to incorporate both viscoelasticity and non-linearity of soft tissue in a robust integro-differential equation. The QLV model is given by

$$\sigma(t) = \int_0^t \left\{ K(t-\tau) \frac{d}{d\tau} \left[\sigma^e(\lambda(\tau)) \right] \right\} d\tau \qquad \text{Equation 23}$$

where σ is the stress, λ is the stretch, σ^e is the elastic response, and $K(t)$ is the reduced relaxation function. Fung proposed $K(t)$ as

$$K(t) = \frac{1 + c \int_{\tau_1}^{\tau_2} \frac{1}{\tau} \exp\left(-\frac{t}{\tau}\right) d\tau}{1 + c \ln\left(\frac{\tau_2}{\tau_1}\right)} \qquad \text{Equation 24}$$

Despite the QLV model being more difficult to implement than most differential models, many authors suggest that the QLV model produces more accurate results and accounts for the non-linear behavior of soft tissue over a continuous spectrum of stress relaxation times. Therefore, it is recommended for future improvement of the system to investigate the use of the QLV model to predict the non-linear behavior of soft tissue.

The prototyped system was used by a physician to perform as set of measurements on six patients which were given the following identifiers to conceal their true identity: DR, JS, CS, KD, RC, and RG. Out of six patients, two (RC and RG) had some degree of prolapse while the other four had no prolapse. As discussed in previous chapters, the test parameters can be customized by the physician, namely the angles of motions and timings. The tests were conducted using three different angle schemes of 10, 15, and 20 degrees of rotation of the finger joint. Additionally, they were conducted using two different timing schemes of 1-1-1 and 1-6-1, where the numbers translate to indentation-hold-release times. There were 6 tests per patient, adding up to 36 tests, see Figure 4.6. The system was also programmed to repeat each test three times to account for any abnormalities. The research aims to explore the feasibility of using the loading data during the indentation period to obtain a characteristic measure of the tissue viscoelastic behavior, see Figure 4.7.
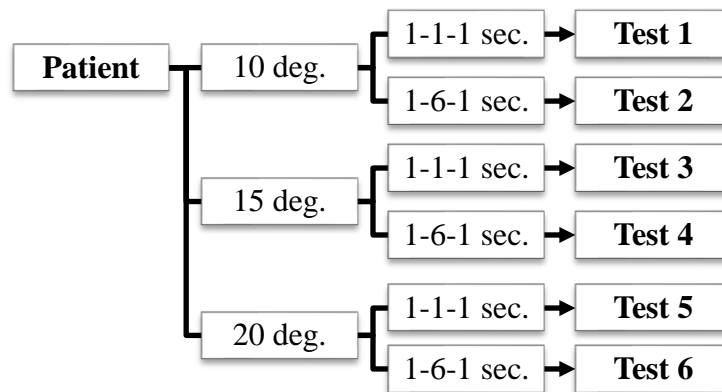
Figure 4.6 – Order of the tests conducted on each patient

Some individual tests exhibited the symptoms predicted from the sensor characterization, where the sensor retains some of the applied load due to the preload. For the same test parameters,

it was clear that the sensor baseline and reading were rising as the test was repeated. For example, the average standard deviation of the test shown in Figure 4.7 was 0.011V or 16% of the test range. While not all tests have exhibited this issue, its presence reduced the confidence in the test results, and highlighted the need for a more repeatable sensor. Nonetheless, some of the tests were more repeatable. For example, the average standard deviation of the test conducted on JS, shown in Figure 4.8, was 0.005V or 4.6% of the test range.
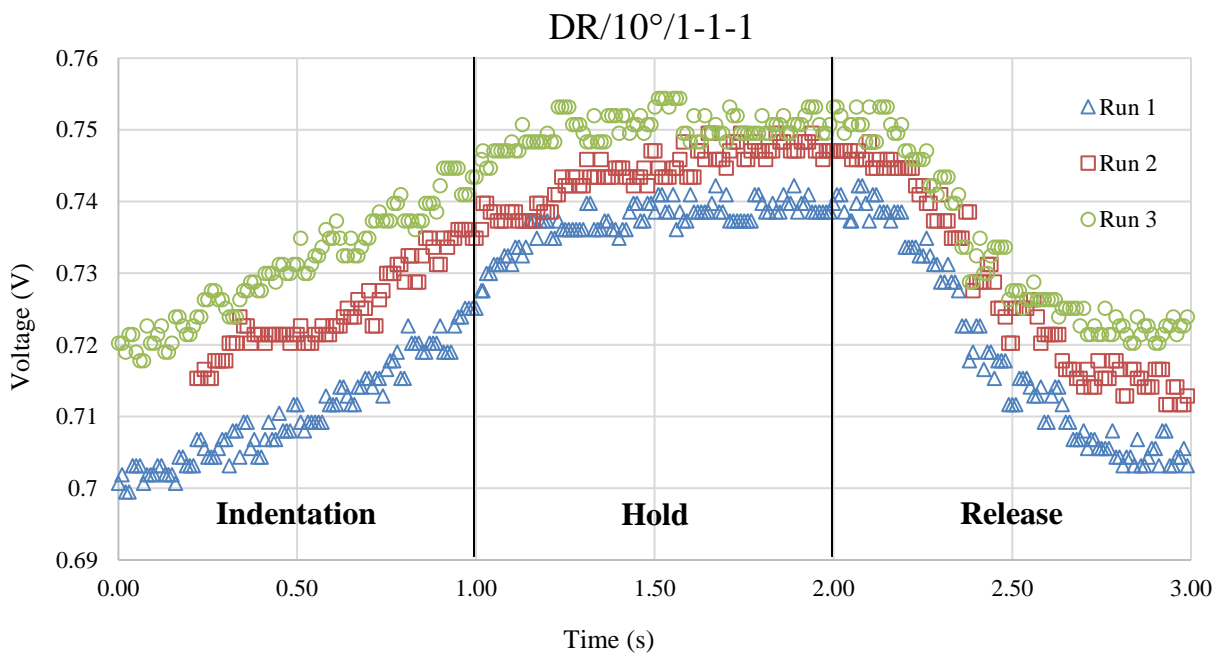
Figure 4.7 – Test data (overlaid) for DR using 10° rotation and 1-1-1s timing. The sensor exhibits load retention as the test is repeated.
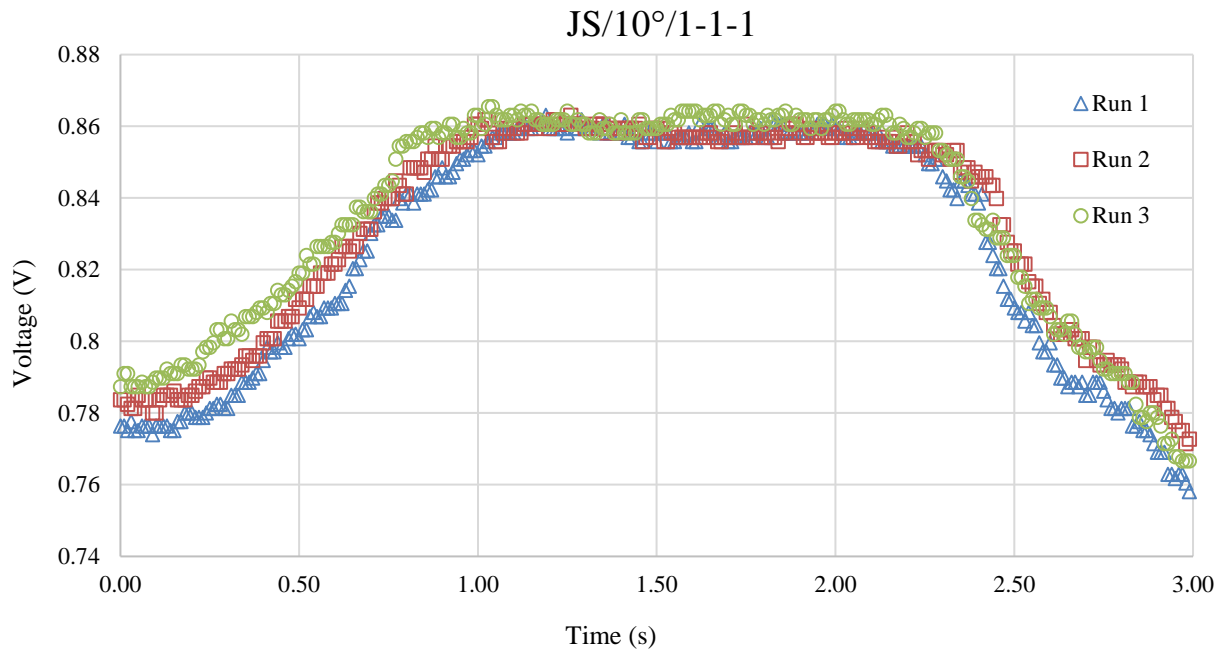
Figure 4.8 – Test data (overlaid) for JS using 10° rotation and 1-1-1s timing

Comparing the different tests, it was observed that the sensor voltage output in the hold period increases as the indentation angle increases as expected. However, as apparent in Figure 4.9, it was also noted that the sensor baseline often differs between tests for the same patient. This observation again raised questions whether any conditions changed between tests (the device was moved, the patient shifted, etc.), or whether the sensor retained any load, or both. This uncertainty in the sensor data prevents an accurate comparison between test results.

For the purpose of conducting the analysis, it is possible to disregard the sensor errors, and assume that the shift in baseline is only due tos a difference between testing conditions. Then, the curves can be normalized by subtracting the lowest baseline value from each data point. This normalization effectively reduces the baseline of all the curves to zero. Furthermore, rather than comparing the maximum voltage value, a more accurate measure of the difference in tissue behavior between the curves/tests is the time constant τ.
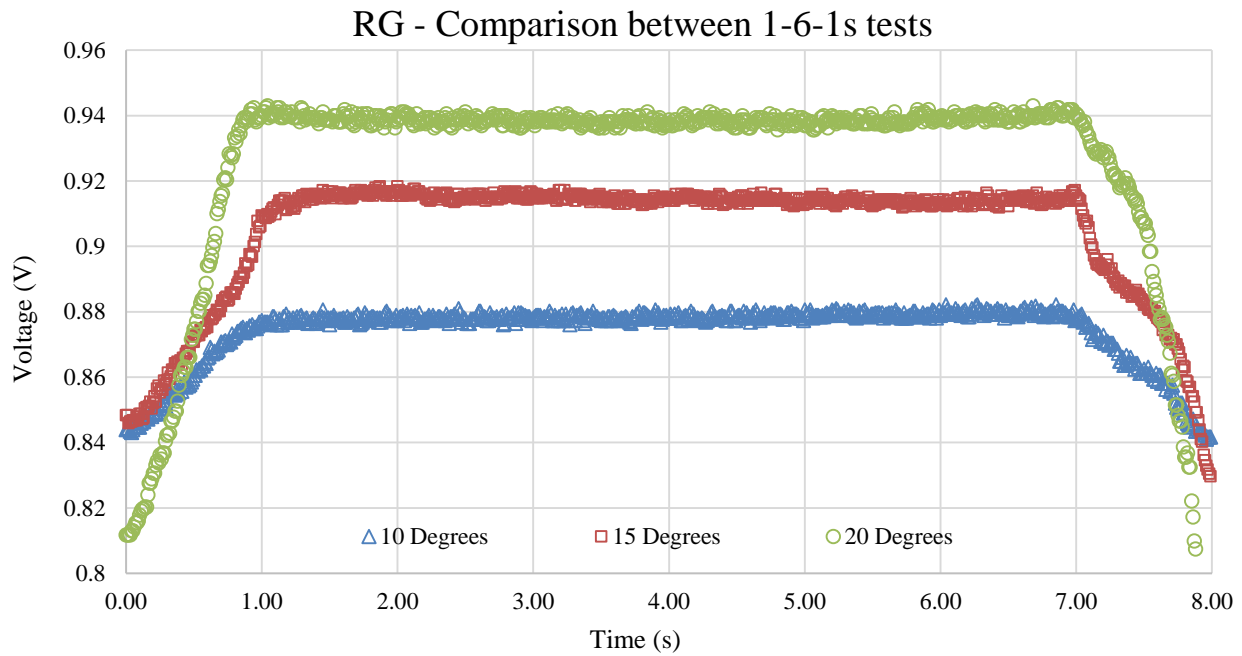
Figure 4.9 – Comparison between test data for RG using 1-6-1s timings and 3 different angles

As discussed in the previous subsection "Viscoelastic Modeling", the time constant is a measure of the viscoelastic behavior of the tissue. A high time constant indicates high damping effects in the tissue, and as such the tissue takes longer time to respond to the force and vice-versa. A linear viscoelastic material should have the same time constant regardless of the strain rate or stress-strain history in general, considering that all testing conditions remain the same. On the other hand, a non-linear viscoelastic material would exhibit a change in the response time between different strain histories.

The data was curve-fit using the Maxwell model discussed in the previous section. The curve-fit was based on minimizing the Root Mean Square Error (RMSE) between the model curve and the experimental data which can be seen in Figure 4.10. Two important observations can be made. First, the Maxwell model is effective to a certain extent in completing the curve-fitting task

accurately. For instance, the RMSEs for the 10, 15 and 20 degree curve-fits are 0.005V, 0.006V

and 0.006V respectively. This corresponds to 6.9%, 5.1% and 4.6% of the final value. Second,

based on the curve-fits using the Maxwell model, the time constant differs between different strain

rates for the same patient.
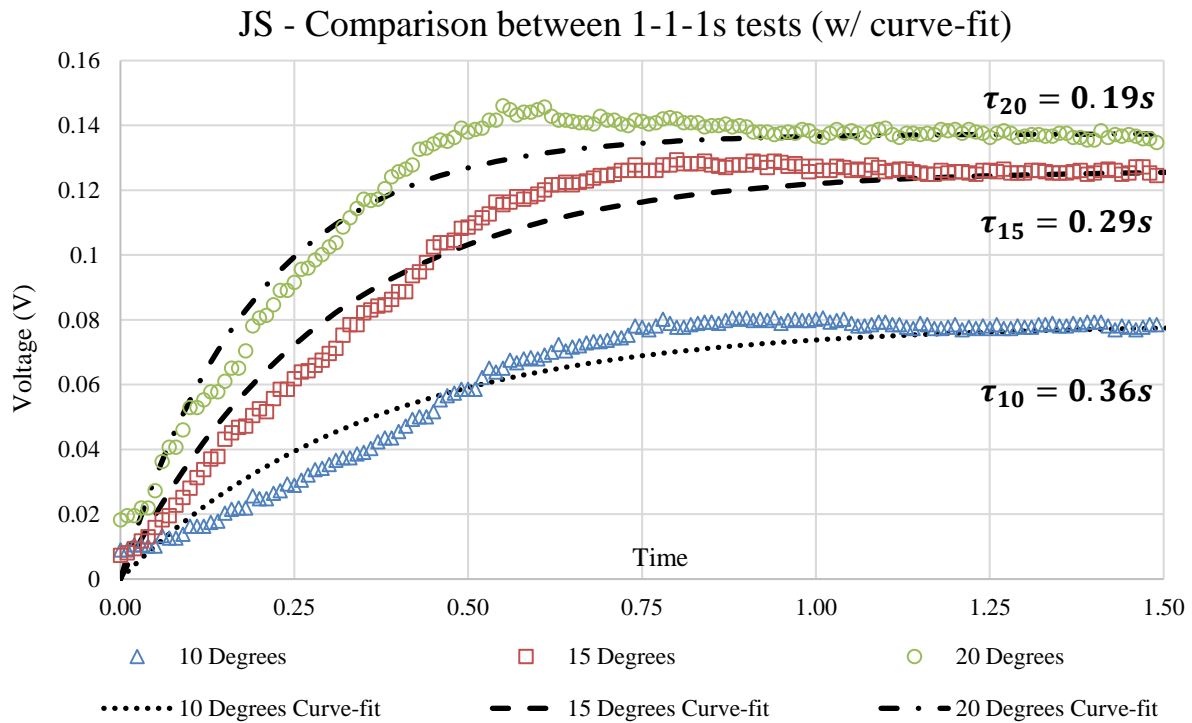
Figure 4.10 – Comparison between test data for JS using 1-1-1s timings and 3 different angles

(with curve-fitting included)

This result was expected due to the fact that soft tissue is a non-linear viscoelastic material

while the Maxwell model is a linear model. This latter observation also alludes to the fact that

using a non-linear viscoelastic model is recommended for future improvements to the system

Finally, a shortcoming of the sensor which was overserved in the test data is the fact that

the sensor load retention may be causing the loss of the force relaxation profile. During the hold

period of the test, the tissue was expected to relax and the reaction force to slowly decrease from

the value reached after indentation. Conversely, the sensor signal was found to be rising slightly as it settles, see Figure 4.11. This can be explained by the sensor retaining some of the applied load and continuing to settle during the hold period. It may be beneficial with future tests to investigate whether this trend will persist during longer hold times such as 20 or 30 seconds.

DR/10°/1-6-1 - Hold time only
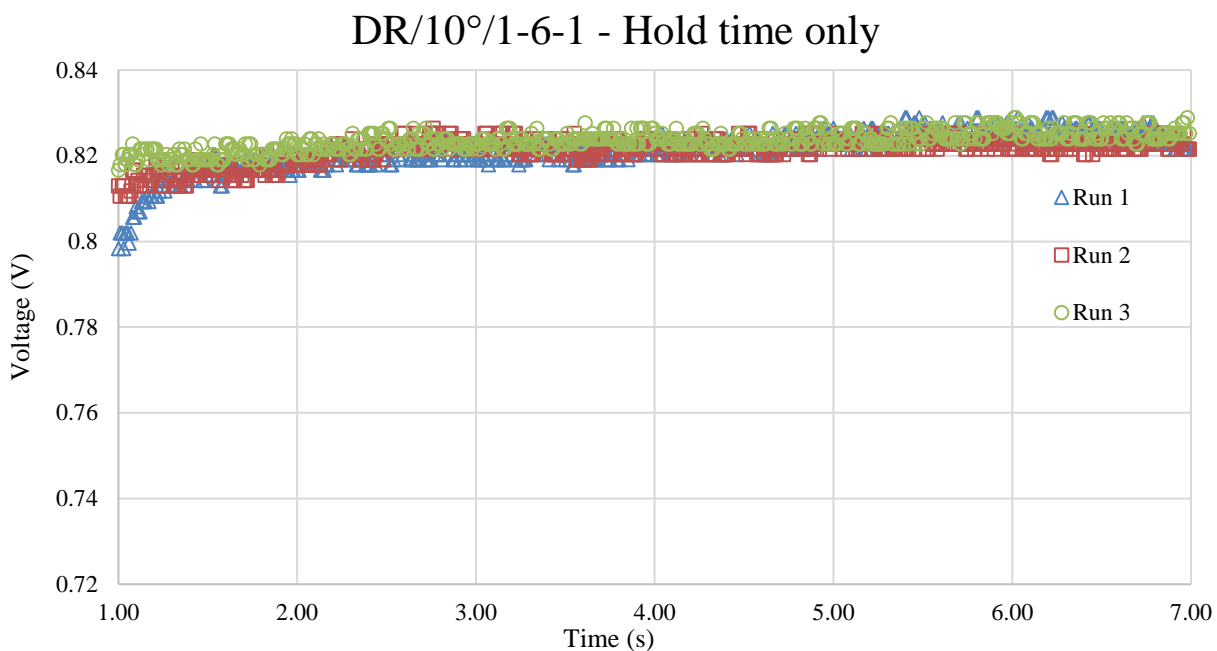
Figure 4.11 – Hold time graph for DR using 10° rotation and 1-6-1s timings

In summary, the in-vivo test data has proven the feasibility of the system in obtaining force-time data from the patients given a specific indentation profile, as well as the feasibility of using this data to characterize the viscoelastic behavior of the vaginal tissue. This characterization can later be correlated to certain factors or conditions, such as age, childbirth, or others, that may adversely affect the soft tissue. However, the shortcomings of the FSR sensor, namely the relatively slow response and the load retention, have posed a challenge to putting confidence in the obtained data. Therefore, the test data have also emphasized the need for using a more reliable sensor.

Chapter 5

CONCLUSIONS AND RECOMMENDATIONS

<u>Conclusions</u>

The goal of the research presented in this thesis was to design and prototype a system for testing vaginal soft tissue in-vivo which is: minimally invasive, automated, repeatable, user-friendly, and capable of automated data processing. The principle of operation is that the system applies a desired indentation/displacement profile on the soft tissue using an actuator, while simultaneously recording the resulting force profile using a force sensor. This force profile is automatically curve-fit to a given viscoelastic model to characterize the tissue and evaluate a quantitative measure of its biomechanical condition.

After multiple iterations, the mechanical design of a Smart Finger probe was synthesized, with design features to ensure the safety and comfort of the patients. Most importantly, the design incorporates an easily removable and replaceable fingertip. This feature provides a flexible method of using different sensing technologies, applying future improvements, and replacing faulty sensors.

The designed Smart Finger and supporting components were prototyped using 3D-printing technology, while load-bearing support structures were fabricated in the University of Texas at Arlington Machine Shop.

The sensor used, a force sensitive resistor, was calibrated using dead weights and a custom calibration rig. The calibration revealed potential shortcomings of the FSR sensor which were not clearly obvious from the sensor manufacturer data sheet; first, the sensor possessed a "dead zone" where no load can be measured below a threshold load; second, when the sensor is preloaded to

overcome this limitation, it becomes unable to completely release any additional load applied to it, which causes the sensor baseline and readings to shift with repeated usage; and third, the sensor response was found to be somewhat slower than desired, with the settling time reaching an average of 0.84s. These limitations highlighted the need for using a more reliable sensor.

The actuator used, a DC-motor/encoder combo, was controlled using PWM and digital PID control scheme. An electronic circuit was created to integrate both the sensor and actuator into the controller. The controller, an NI myRIO, was used as an interface between hardware and software. Additionally, NI LabVIEW was used to create the graphical user interface to enable the user to input the testing parameters, namely the indentation angle and the motion timings.

Finally, the prototyped system was tested in-vivo on six patients with both prolapsed and non-prolapsed vaginal canal. The tests demonstrated the viability of the developed system, and helped verify the soundness of the design and prototype. However, the tests also showed the shortcomings of the sensor, which causes some uncertainty in the data obtained and in the characterization parameters analyzed.

In summary, the characteristics of the system were attained to the following degrees:

- Minimally invasive: the system operates similar to a regular pelvic exam, and causes minimal discomfort to the patient.

- Automated: the system requires input of the test parameters by the user, as well as positioning the Smart Finger in the vaginal canal before testing. Apart from these two requirements, the test is carried out automatically and without the need for any further user action.

- Repeatable: the motion of the finger joint is repeatable. However, the force sensor signal can include some errors. Additionally, the initial position of the Smart Finger within the vaginal canal is controlled by the user, which can decrease repeatability to some extent.

- User-friendly: the system has a GUI which simplifies the test procedure significantly, and allows for test parameter customization. The hardware is also portable and relatively easy to adjust using the tripod. The Smart Finger probe can be covered with a flexible cover/boot which negates the need for repeated sterilization.

- Capable of automated data modeling: a preliminary algorithm for automated data modeling was created. However, it was not used on the collected data sets due to the errors observed in the data, and the need for further fine-tuning of the data modeling program.

All future improvements to the system should aim to maximize these aforementioned characteristics.

Recommendations

A crucial improvement is upgrading the sensor. The current FSR sensor has the distinct advantage of being very compact and low-profile. However, it is lacking in important performance metrics such as response time, repeatability, and the existence of a "dead zone". It is suggested to investigate other sensor technology (load cells, capacitive sensors, or piezoresistive sensors) that might address the shortcomings of the FSR and replace the FSR with one of these sensing technologies. Minimizing sensor error will highly reduce the uncertainty in the test data and help future studies target other possible testing errors such patient movement or structural vibration.

Another important improvement is the choice and implementation of a non-linear viscoelastic model to the system software. The current software curve-fits the test data using a

linear viscoelastic Maxwell Model. However, this model is not fully equipped for recreating the non-linear behavior of biological soft tissue. It is recommended to employ a more suitable model from literature or perform extensive research to synthesize an original vaginal tissue model. This model then needs to be implemented in the LabVIEW software.

In order to test the proposed models for accuracy and sensitivity to different paraments, it is recommended to construct or purchase a testing setup emulating the soft tissue of the vaginal wall. Some viscoelastic materials such as Polydimethylsiloxane (PDMS) can be used to construct a model of the vagina, where the finger can be tested using design of experiments. This can help determine the sensitivity of the force response to variables such as the indentation depth, the strain rate, the fingertip size, the insertion angle, etc. The end result can be a more inclusive viscoelastic model that accounts for more of the test variables, and characterizes the vaginal tissue more accurately.

It is recommended to decrease the diameter of the Smart Finger to a range of 8mm to 12mm. This improvement further reduces the impact of the Smart Finger on the patient: a smaller diameter causes less discomfort when the finger is inserted into the patient. On the other hand, a smaller fingertip diameter exerts higher pressure on the tissue; therefore, careful monitoring of the applied pressure should be conducted.

On the same note, the smaller diameter can be achieved using more compact actuation and power transmission methods, such as a linear motor with cams, a linear motor with a 4 bar linkage, a rotational motor with cables, etc. More compact actuators also increase portability for the user. However, each one of these actuation methods offer advantages and limitations. For instance, a cable drive is more difficult to assemble and maintain than a belt drive, and can also suffer from

loss of tension like the belt drive. A cam mechanism can surpass the loss of tension, but it is more difficult to prototype and more susceptible to friction.

Finally, a possible improvement is the automation of the positioning of the device. Currently, the user needs to position the device manually inside the vaginal canal. Gradations have been created on the Smart Finger to help determine the insertion depth. A more automated version of the system can be designed to accurately insert the Smart Finger to a given depth. Moreover, it can be programmed to use the sensor data to center the finger within the vaginal canal before testing. All these improvements can help increase the repeatability of the device.

References

[1] M. George Lazarou, "Pelvic Organ Prolapse," 20 6 2016. [Online]. Available: http://emedicine.medscape.com/article/276259-overview.

[2] W. Jennifer M, H. Andrew F, F. Rebekah G and M. Evan R., "Forecasting the prevalence of pelvic floor disorders in U.S. Women: 2010 to 2050," *Obstet Gynecol,* vol. 114, no. 6, pp. 1278-83, 2009.

[3] A. L. Olsen, V. J. Smith, J. O. Bergstrom, J. C. Colling and A. L. Clark, "Epidemiology of surgically managed pelvic organ prolapse and urinary incontinence," *Obstetrics & Gynecology,* vol. 89, pp. 501-506, 1997.

[4] S. Swift, P. Woodman, A. O. Boyle, M. Kahn, M. Valley, D. Bland, W. Wang and J. Schaffer, "Pelvic Organ Support Study (POSST): The distribution , clinical definition , and epidemiologic condition of pelvic organ support defects," *American Journal of Obstetrics and Gynecology,* vol. 192, pp. 795-806, 2005.

[5] "WebMD," Healthwise, Inc, 12 March 2014. [Online]. Available: http://www.webmd.com/women/uterine-prolapse.

[6] C. J. Chuong, M. Ma, P. Zimmern and R. C. Eberhart, "European Journal of Obstetrics & Gynecology and Reproductive Biology Viscoelastic properties measurement of the prolapsed anterior vaginal wall : a patient-directed methodology," *European Journal of Obstetrics and Gynecology,* vol. 173, pp. 106-112, 2014.

[7] F. J. Carter, T. G. Frank, P. J. Davies, D. McLean and A. Cuschieri, "Measurements and modelling of the compliance of human and porcine organs," *Medical Image Analysis,* vol. 5, pp. 231-236, 2001.

[8] K. Miller, K. Chinzei, G. Orssengo and P. Bednarz, "Mechanical properties of brain tissue in-vivo: Experiment and computer simulation," *Journal of Biomechanics,* vol. 33, pp. 1369-1376, 2000.

[9] B. Ahn and J. Kim, "Measurement and characterization of soft tissue behavior with surface deformation and force response under large deformations," *Medical Image Analysis,* vol. 14, pp. 138-148, 2010.

[10] H. Liu, D. P. Noonan, Y. H. Zweiri, K. A. Althoefer and L. D. Seneviratne, "The development of nonlinear viscoelastic model for the application of soft tissue identification," *2007 IEEE/RSJ International Conference on Intelligent Robots and Systems,* pp. 208-213, 2007.

[11] H. Liu, K. Sangpradit, M. Li, P. Dasgupta, K. Althoefer and L. D. Seneviratne, "Inverse finite-element modeling for tissue parameter identification using a rolling

indentation probe," *Medical and Biological Engineering and Computing,* vol. 52, pp. 17-28, 2014.

[12] E. Samur, M. Sedef, C. Basdogan, L. Avtan and O. Duzgun, "A robotic indenter for minimally invasive measurement and characterization of soft tissue response," *Medical Image Analysis,* vol. 11, pp. 361-373, 2007.

[13] B. K. Tay, J. Kim and M. a. Srinivasan, "In vivo mechanical behavior of intra-abdominal organs," *IEEE Transactions on Biomedical Engineering,* vol. 53, pp. 2129-2138, 2006.

[14] M. Cosson, E. Lambaudie, M. Boukerrou, P. Lobry and G. Cre, "A biomechanical study of the strength of vaginal tissues Results on 16 post-menopausal patients presenting with genital prolapse," *European Journal of Obstetrics & Gynecology and Reproductive Biology,* vol. 112, pp. 201-205, 2004.

[15] E. Peña, P. Martins, T. Mascarenhas, R. M. N. Jorge, A. Ferreira, M. Doblaré and B. Calvo, "Mechanical characterization of the softening behavior of human vaginal tissue," *Journal of the Mechanical Behavior of Biomedical Materials,* vol. 4, pp. 275-283, 2011.

[16] C. Rubod, M. Boukerrou, M. Brieu, C. Jean-charles, P. Dubois and M. Cosson, "Biomechanical properties of vaginal tissue : preliminary results," *International Urogynecology Journal,* vol. 19, pp. 811-816, 2008.

[17] H. van-Raalte and V. Egorov, "Characterizing female pelvic floor conditions by tactile imaging," *International Urogynecology Journal,* vol. 26, no. 4, p. 607–609, 2015.

[18] M. E. Cronemiller, "Artificial arm and hand". US Patent 1,225,415, 8 May 1917.

[19] R. A. Brookhuis, T. S. J. Lammerink, R. J. Wiegerink, D. a. M. J. Boer and M. C. Elwenspoek, "3D force sensor for biomechanical applications," *Sensors and Actuators, A: Physical,* vol. 182, pp. 28-33, 2012.

[20] G. Liang, Y. Wang, D. Mei, Kailun and Z. Chen, "Flexible Capacitive Tactile Sensor Array With Truncated Pyramids as Dielectric Layer for Three-Axis Force Measurement," *Journal of Microelectromechanical Systems,* vol. 24, pp. 1510-1519, 2015.

[21] Y. Jung, D. G. Lee, J. Park, H. Ko and H. Lim, "Piezoresistive tactile sensor discriminating multidirectional forces," *Sensors,* vol. 15, pp. 25463-25473, 2015.

[22] Q. Liang, W. Wang, D. Zhang, Y. Ge and X. Huang, "Miniature robust five-dimensional fingertip force / torque sensor with high performance," *Measurement Science and Technology,* vol. 22, 2011.

[23] "NCI Dictionary of Cancer Terms," National Cancer Institute, [Online]. Available: https://www.cancer.gov/publications/dictionaries/cancer-terms?cdrid=322873.

[24] Y. Hsu, L. Chen and J. O. L. Delancey, "Vaginal Thickness, Cross-Sectional Area, and Perimeter in Women With and Those Without Prolapse Yvonne," *Obstet Gynecol,* vol. 105, pp. 1012-1017, 2005.

[25] G. Langevin, "InMoov," [Online]. Available: https://inmoov.fr/finger-starter/.

[26] S.-H. Ahn, M. Montero, D. Odell, S. Roundy and P. K. Wright, "Anisotropic material properties of fused deposition modeling ABS," *Rapid Prototyping Journal,* vol. 8, pp. 248-257, 2002.

[27] N. L. Hoekstra, B. P. Kraft and J. L. Newcomer, "Effect of Layer Orientation on the Mechanical Properties of Acrylonitrile-Butadiene-Styrene Test Specimens Produced by Fused Deposition Modeling," *Journal of Injection Molding Technology,* vol. 5, pp. 193-199, 2001.

[28] J. F. Rodríguez, J. P. Thomas and J. E. Renaud, "Mechanical behavior of acrylonitrile butadiene styrene fused deposition materials modeling," *Rapid Prototyping Journal,* vol. 9, pp. 219-230, 2003.

[29] "FSR 400," Interlink Electronics, Inc., [Online]. Available: http://www.interlinkelectronics.com/FSR400.php.

[30] "Coreless DC Motors - Data Sheets," Micromo, [Online]. Available: http://www.micromo.com/products/dc-motors/coreless-dc-motors-data-sheets.

[31] S. D. Abramowitch, "An Improved Method to Analyze the Stress Relaxation of Ligaments Following a Finite Ramp Time Based on the Quasi-Linear Viscoelastic Theory," *Journal of Biomechanical Engineering,* vol. 126, p. 92, 2004.

[32] L. Han, J. A. Noble and M. Burcher, "A novel ultrasound indentation system for measuring biomechanical properties of in vivo soft tissue," *Ultrasound in Medicine and Biology,* vol. 29, pp. 813-823, 2003.

[33] M. Kauer, V. Vuskovic, J. Dual, G. Szekely and M. Bajka, "Inverse finite element characterization of soft tissues," *Medical Image Analysis,* vol. 6, pp. 275-287, 2002.

[34] A. Nava, E. Mazza, M. Furrer, P. Villiger and W. H. Reinhart, "In vivo mechanical characterization of human liver," *Medical Image Analysis,* vol. 12, pp. 203-216, 2008.

[35] A. Nekouzadeh, K. M. Pryse, E. L. Elson and G. M. M. Genin, "A simplified approach to quasi-linear viscoelastic modeling," *Journal of Biomechanics,* vol. 40, pp. 3070-3078, 2007.

[36] J. J. Sarver, "Methods for Quasi-Linear Viscoelastic Modeling of Soft Tissue: Application to Incremental Stress-Relaxation Experiments," *Journal of Biomechanical Engineering,* vol. 125, p. 754, 2003.

[37] F. Xu, K. Seffen and T. Lu, "A Quasi-Linear Viscoelastic Model for Skin Tissue," in *Proceedings of the 3rd IASME / WSEAS International Conference on Continiuum Mechanics (CM'08)*, 2008.

[38] M. Kohandel, S. Sivaloganathan and G. Tenti, "Estimation of the quasi-linear viscoelastic parameters using a genetic algorithm," *Mathematical and Computer Modelling,* vol. 47, pp. 266-270, 2008.

[39] Y. J. Lim, D. Deo, T. P. Singh, D. B. Jones and S. De, "In situ measurement and modeling of biomechanical response of human cadaveric soft tissues for physics-based surgical simulation," *Surgical Endoscopy and Other Interventional Techniques,* vol. 23, pp. 1298-1307, 2009.

Biographical Information

Michael Abraham was born in Cairo, Egypt, in 1990. He completed three years of Mechanical Engineering in Ain Shams University at Cairo, with the intended specialty of Mechatronics Engineering. In 2012, he transferred his studies to the University of Texas at Arlington in the United States, where he received his B.Sc. in Mechanical Engineering in 2014, and later his M.Sc. in Mechanical Engineering in 2016. His research interests include machine design, robotics, automation, and control. He plans to pursue these interests especially in the biomedical field, and emerging fields such as human-robot interaction, virtual reality, and autonomous vehicles.